J Neurophysiol 108: 1106–1121, 2012.
First published May 9, 2012; doi:10.1152/jn.01034.2011.

Differential coding by two olfactory subsystems in the honeybee brain

Julie Carcaud,[1,2,3] Thomas Hill,[1,2] Martin Giurfa,[1,2] and Jean-Christophe Sandoz[3]

[1]*Université de Toulouse (UPS), Centre de Recherches sur la Cognition Animale, Toulouse Cedex, France;* [2]*Centre National de la Recherche Scientifique (CNRS), Centre de Recherches sur la Cognition Animale, Toulouse Cedex, France; and* [3]*Evolution, Genomes and Speciation Lab, CNRS (UPR 9034), Gif-sur-Yvette Cedex, France*

Submitted 14 November 2011; accepted in final form 7 May 2012

Carcaud J, Hill T, Giurfa M, Sandoz JC. Differential coding by two olfactory subsystems in the honeybee brain. *J Neurophysiol* 108: 1106–1121, 2012. First published May 9, 2012; doi:10.1152/jn.01034.2011.— Sensory systems use parallel processing to extract and process different features of environmental stimuli. Parallel processing has been studied in the auditory, visual, and somatosensory systems, but equivalent research in the olfactory modality is scarce. The honeybee *Apis mellifera* is an interesting model for such research as its relatively simple brain contains a dual olfactory system, with a clear neural dichotomy from the periphery to higher-order centers, based on two main neuronal tracts [medial (m) and lateral (l) antenno-protocerebral tract (APT)]. The function of this dual system is as yet unknown, and attributes like odor quality and odor quantity might be separately encoded in these subsystems. We have thus studied olfactory coding at the input of both subsystems, using in vivo calcium imaging. As one of the subsystems (m-APT) has never been imaged before, a novel imaging preparation was developed to this end, and responses to a panel of aliphatic odorants at different concentrations were compared in both subsystems. Our data show a global redundancy of olfactory coding at the input of both subsystems but unravel some specificities for encoding chemical group and carbon chain length of odor molecules.

olfaction; parallel processing; optical imaging; insect

SENSORY STIMULI often exhibit multiple features that can be segregated by the central nervous system, which processes them through parallel pathways prior to later integration stages. Such strategy has been convincingly demonstrated in the auditory (Rauschecker and Tian 2000), somatosensory (Reed 2005), and visual (Livingston and Hubel 1988; Strausfeld and Lee 1991; Yamaguchi et al. 2008) systems. For instance, in the vertebrate brain, a ventral pathway conveys information from the primary visual cortex (V1) to the infero-temporal cortex and is associated with the processing of form, color, and object representation, and is therefore termed the "What" pathway. In parallel, a dorsal pathway leads information from V1 to the dorso-medial cortex, processes movement and object localization, and corresponds to a "Where" pathway (Ettlinger 1990). In the olfactory modality, a dichotomy of odor processing appears in the form of a sex pheromone-specific subsystem and a general odor coding subsystem, both in vertebrates (Dulac and Wagner 2006) and in insects (Datta et al. 2008; Hansson and Anton 2000; Mustaparta 1996). However, such dedicated subsystems segregate odorants according to their biological value rather than to specific chemical features of odor molecules. Olfaction is highly complex in the sense that odor molecules may differ in many characteristics such as functional group, chain length, saturation, and three-dimensional structure, among others, which could be the object of specific processing in the nervous system (Haddad et al. 2008; Johnson and Leon 2007; Mori 2006). Efficient olfactory systems may need to recognize an odorant irrespective of its concentration but also to monitor absolute odor concentration in order to find an odor source (Asahina et al. 2009; Uchida and Mainen 2007). In addition, recognition of an odor mixture irrespective of fluctuations in its constituents (configural perception), discrimination between very similar mixtures, or recognition of particular components within a mixture (elemental perception) may rely on differential processing of olfactory information (Derby 2000; Riffel et al. 2009; Uchida and Mainen 2007).

Parallel olfactory pathways are a common trait in insect olfactory systems, with the highest level of complexity in Blattaria, Diptera, and especially Hymenoptera (Galizia and Rössler 2010). Among the latter, the honeybee *Apis mellifera L.* represents an ideal model for the study of parallel olfactory processing, as its neural circuits have been extensively described (Abel et al. 2001; Kirschner et al. 2006) and are accessible to electrophysiology (Abel et al. 2001; Krofczik et al. 2009; Müller et al. 2002) or optical imaging (Galizia and Menzel 2001). In honeybees (Fig. 1*A*), odors are detected by olfactory receptor neurons (ORNs, ~60,000; Esslen and Kaissling 1976) on each antenna that project to a primary olfactory center, the antennal lobe (AL), the equivalent of the vertebrate olfactory bulb (Hildebrand and Shepherd 1997). Within the AL's 160 anatomical and functional units, the glomeruli, ORNs synapse with ~4,000 local interneurons carrying out local computations and with ~800 projection neurons (PNs). PNs further convey the reshaped olfactory information to higher brain centers, the mushroom bodies (MBs) and the lateral horn (LH), via different neural tracts. In particular, two nonoverlapping subsets of AL glomeruli send their information separately to the MB and the LH, thereby providing the basis for a dual olfactory system (Abel et al. 2001; Kirschner et al. 2006; Müller et al. 2002). About half of the glomeruli use the lateral antenno-protocerebral tract of PNs (l-APT, 84 glomeruli) while the other half use the medial tract (m-APT, 77 glomeruli). Within the MB calyces but also in the LH, PNs from each tract project to nonoverlapping areas (Kirschner et al. 2006). As far as we know in insects, sensory neurons carrying a particular type of olfactory receptor protein project to the same glomerulus (Vosshall et al. 2000). One may thus say that PNs from the l- and m-APT each transmit information about two independent portions of the honeybee odor detection repertoire. Therefore, the neural architecture of the honeybee olfactory system suggests that olfactory information could be conveyed and processed separately by the l-APT and m-APT

Address for reprint requests and other correspondence: J.-C. Sandoz, Evolution, Genomes and Speciation Lab, CNRS (UPR 9034), 1 Ave. de la Terrasse, 91198 Gif-sur-Yvette cedex, France (e-mail: sandoz@legs.cnrs-gif.fr).

subsystems, with possibly different functions. Whether these two subsystems code odor information redundantly or differentially is still controversial (Galizia and Rössler 2010).

In vivo calcium imaging studies showed that odors are encoded at the level of the AL as glomerular activity patterns (Deisig et al. 2006, 2010; Galizia et al. 1999b; Joerges et al. 1997; Sachse et al. 1999; Sachse and Galizia 2002, 2003; Sandoz 2006). Furthermore, odors inducing similar glomerular activity patterns are treated by bees as similar in behavioral generalization tests (Guerrieri et al. 2005). However, all previous calcium imaging studies on honeybee olfactory coding at the level of the AL have focused on the l-APT subsystem, as these glomeruli are directly optically accessible when the head capsule is opened (see Galizia and Vetter 2005). By contrast, glomeruli of the m-APT subsystem are hidden on the posterior side of the AL so that little is known about how the m-APT subsystem represents odors. An electrophysiological study initially reported that m-APT neurons code odors by latency differences and l-APT neurons by spike rate differences (Müller et al. 2002), yet later recordings could not confirm this finding and instead suggested a difference in mixture processing (Krofczik et al. 2009). In addition, a calcium imaging study compared the responses of anterogradely stained PN boutons of both subsystems in the MB calyx (Yamagata et al. 2009) and suggested a functional division of the two subsystems, with respect to concentration and mixture processing. In this study, m-APT neurons showed a clearer dependence on odor concentration, a broader odor-response profile, and less antagonistic mixture effects than l-APT neurons. This work also showed that the recorded responses were shaped by presynaptic GABAergic inhibition so that it is unclear whether the observed odor response differences are inherited from peripheral coding and/or AL processing or are a product of MB microcircuits (Schmuker et al. 2011; Yamagata et al. 2009).

In the present work we performed calcium imaging recordings after bath application of a calcium-sensitive dye in the bee brain in order to study possible functional differences between the l- and m-APT subsystems. In this way, we recorded a compound signal dominated by sensory input (Deisig et al. 2010; Galizia et al. 1998; Sachse and Galizia 2003) that allowed comparison of odor coding at the input level of the AL between the l- and m-APT subsystems. This approach is necessary to determine whether differences between both subsystems are already present in the different subsets of ORNs innervating them. Since odor-evoked activity from glomeruli belonging to the m-APT subsystem could never be recorded, we developed a preparation that allows imaging the AL from the posterior brain surface. Using this and the traditional preparation allowing imaging of the l-APT subsystem, we explored odor quality and quantity coding in m-APT and l-APT glomeruli. We presented a set of 16 aliphatic odors differing in their functional groups and/or carbon chain lengths and determined the extent to which both subsystems are able to account for odor similarity relationships as established through behavioral generalization experiments (Guerrieri et al. 2005). In another set of experiments, we examined odor quantity coding in both subsystems by presenting three different odorants at eight different concentrations and comparing coding efficiency according to concentration. Our results show that olfactory coding in both m-APT and l-APT subsystems is mostly redundant at the input level of the AL but with a differential specialization in the coding of chain length versus functional group. While functional group is the primary coding dimension in the m-APT subsystem, chain length is primarily coded by the l-APT subsystem.

MATERIALS AND METHODS

Honeybee preparation. Adult *Apis mellifera L.* workers were captured from an indoor hive during the winter or from an outdoor hive during the summer. Honeybees were chilled on ice for 5 min until they stopped moving and were then placed in a Plexiglas recording chamber. The standard preparation for visualizing the glomeruli belonging to the l-APT subsystem was used (Joerges et al. 1997; Sandoz et al. 2003). Briefly, the head was fixed with low-temperature-melting wax to avoid movements. The antennae were oriented to the front with cactus spines and fixed with a two-component glue (red Araldite, Bostik Findley) so that they remained in the air during the experiment and could be stimulated with odors. To create a small pool for saline solution around the brain small pieces of plastic were fixed with wax, and the brain region could be kept in saline solution. A small window was cut in the head cuticle, and glands and trachea were removed to expose the ALs.

A new preparation was developed for visualizing the glomeruli innervated by the m-APT, which are found on the dorsal part of the AL. Honeybees were fixed on their back on a plastic chamber with small pieces of tape. The antennae were passed through a small hole in the bottom of the chamber, so that they could be placed in an airflow for odor presentations. The head was then fixed with low-temperature-melting wax. To create a pool around the brain for keeping it under saline solution, small pieces of plastic were fixed as above with wax. The cuticle on the inferior part of the head was removed, as were the tentorial arms (cuticle pillars within the head capsule; Snodgrass 1956). Glands and trachea were removed to expose the brain. As the subesophageal ganglion (SEG) mostly covers the rest of the brain from this view, it was in part removed to reach the inferior part of ALs.

The brain was regularly rinsed with saline solution (in mM: 130 NaCl, 6 KCl, 4 $MgCl_2$, 5 $CaCl_2$, 160 sucrose, 25 glucose, 10 HEPES, pH 6.7, 500 mosmol/kgH_2O; all chemicals from Sigma-Aldrich, Lyon, France). For staining, the saline solution was gently removed, and the brain was bathed with 20 μl of dye solution (10 μg Calcium Green-2 AM dissolved with 4 μl Pluronic F-127, 20% in dimethyl sulfoxide, all from Molecular Probes, Invitrogen). The bee was left on ice for 45 min, and then the brain was rinsed again thoroughly with saline solution in order to remove extracellular dye.

Calcium imaging. In vivo optical recordings were performed as described elsewhere (Deisig et al. 2006, 2010; Hourcade et al. 2009; Sandoz et al. 2003), with a T.I.L.L. Photonics imaging system (Martinsried, Germany), under an epifluorescence microscope (Olympus BX51WI) with a $\times$10 water-immersion objective (Olympus, UMPlanFL; NA 0.3). The head region was covered with saline solution, and one AL was recorded in each bee. Images were taken with a 640 $\times$ 480 pixel 12-bit monochrome CCD camera (T.I.L.L. Imago) cooled to -12°C. Each measurement consisted of 100 frames at a rate of 5 frames/s (integration time for each frame: 40–60 ms) with 4 $\times$ 4 binning on chip (pixel image size corresponded to 4.8 μm $\times$ 4.8 μm). Odor stimuli were given at the 15th frame for 1 s. Monochromatic excitation light at 475 nm was applied with a monochromator (T.I.L.L. Polychrom IV). The filter set on the microscope was composed of a 505-nm dichroic filter and an LP 515-nm emission filter. A constant clean airstream, into which odor stimuli could be presented, was directed from a distance of 2 cm to the bee's antennae.

For each odor, 5 μl of the odor solution (either pure or diluted in mineral oil—see below) was placed on a filter paper (1 cm^2) inserted in a Pasteur pipette. All odors were obtained from Sigma-Aldrich (Deisenhofen, Germany). As control stimulus, a pipette containing a clean piece of filter paper was used.

In the odor quality experiment, we tested 16 aliphatic odorants belonging to 4 functional group types (primary and secondary alcohols, aldehydes, and ketones) and carrying 4 different carbon chain lengths (6, 7, 8, and 9 carbons). These odorants are parts of floral blends encountered by bees in nature (Knudsen et al. 1993). Some of them are also components of social pheromones used by bees (Free 1987). For a detailed description of the 16 odorants, see Guerrieri et al. (2005, Table 1 therein). The order of odor presentation was randomized between bees. In the odor quantity experiment, we tested three odors (1-hexanol, heptanal, and 2-octanone) at eight different concentrations, from 10^{-7} to 10^{0}. All odorants were dissolved in mineral oil. Odors were always presented in increasing concentration order, from 10^{-7} to 10^{0}, to avoid adaptation phenomena. The control stimulus was a pipette containing a piece of filter paper soaked with 5 μl of mineral oil.

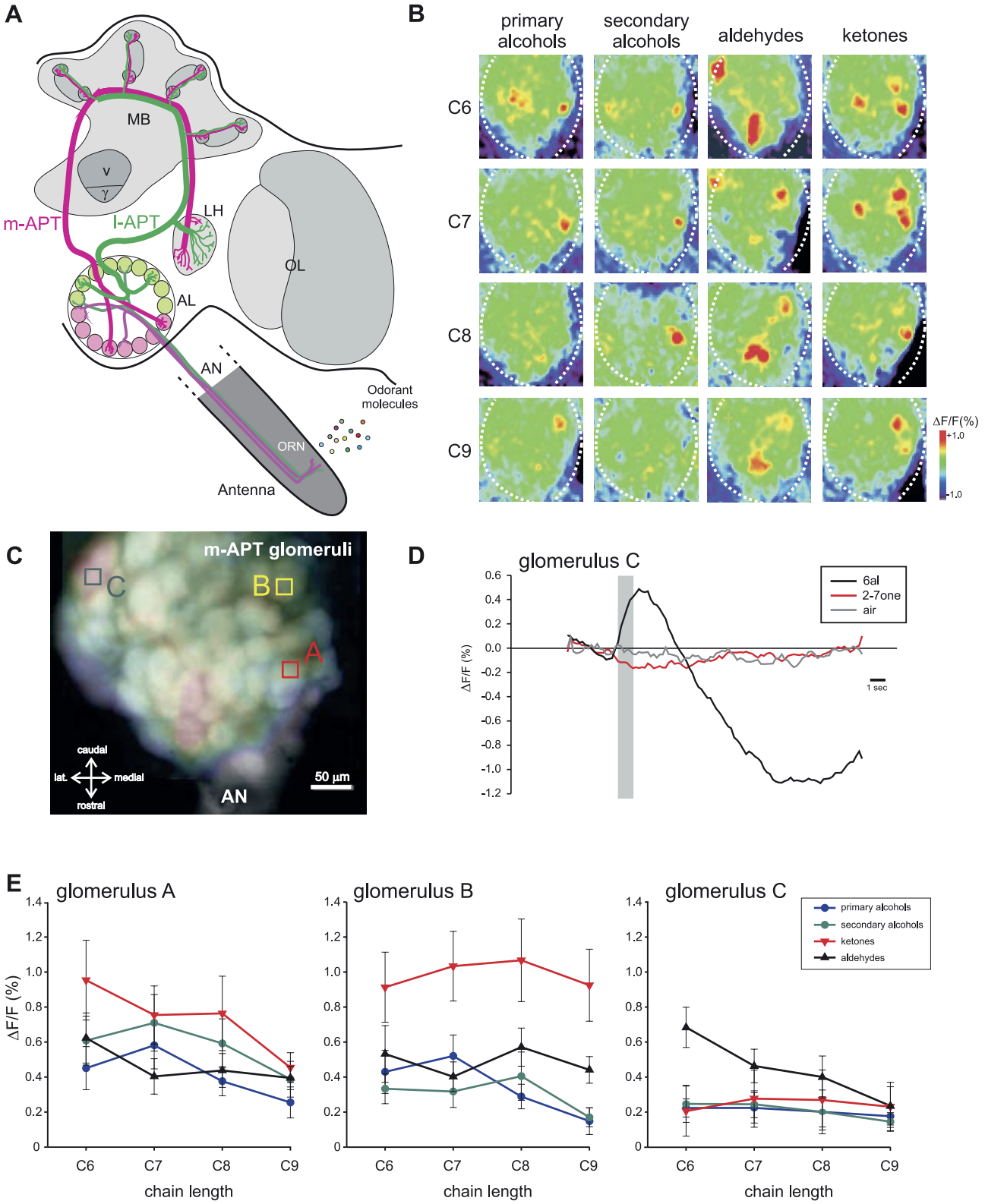

The interval between odor presentations was ~80 s, and three runs with each odorant were done for each bee. Only bees with at least two complete runs were kept for analysis.

Anatomical staining. After calcium imaging experiments, a protease (from *Bacillus licheniformis* in propylene glycol; Sigma-Aldrich) was bath applied in the head capsule for 45 min. The brain was then rinsed with saline, and neutral red solution (Michrome no. 226, Edward Gurr, London, UK, 4% diluted in water) was applied for 20 min. Thereafter, the brain was again carefully washed with saline solution and placed under the microscope exactly as during imaging. With the monochromator at 530-nm excitation light and a filter set composed of a 570-nm dichroic filter and an LP 590-nm emission filter, fluorescence images were taken at 40 different focal planes.

Data processing and analyses. All analyses were carried out with custom-made software written in IDL 6.0 (Research Systems, Boulder, CO). Each recording with an odor stimulus corresponded to a three-dimensional array with two spatial dimensions (*x*, *y* pixels of the region of interest) and a temporal dimension (100 frames). Three steps were carried out to calculate the signals. First, to reduce photon noise, the raw data were filtered in the two spatial and the temporal dimension with a median filter with a size of 3 pixels. Then, taking as reference background F_0 the average of three frames just before any odor stimulation (*frames 12–14*), relative fluorescence changes were calculated as $\Delta F/F = (F - F_0)/F_0$. Finally, to correct bleaching and possible irregularities of lamp illumination in the temporal dimension, a subtraction was made at each pixel of each frame of the median value of all pixels of that frame. A decaying exponential curve was then fitted to this value and subtracted from this frame.

Odor-evoked signals in both parts of the AL (l-APT and m-APT subsystems) presented the typical stereotyped biphasic profile usually obtained with bath-applied Calcium Green, with a fast fluorescence increase followed by a slow decrease below baseline (Fig. 1*D*; Galizia et al. 1997; Sandoz et al. 2003; Stetter et al. 2001). These signals chiefly represent the contribution of afferent ORNs (see Deisig et al. 2010) as they never show any spontaneous activity or inhibitory responses, which are typical for local neurons and PNs (Sachse and Galizia 2002). Therefore the participation of LNs or PNs in the compound signal is thought to be negligible (Galizia and Vetter 2005).

Activity maps are shown with the best possible spatial definition of odor-evoked signals, subtracting the averages of three frames between two time points. The full signal amplitude of the biphasic signal was used, from the maximum around *frame 20* to the minimum around *frame 60*. For the quantification of response intensity and similarity relationships among odors, a Gaussian filter (7 × 7 pixels) was applied on the data. A mask was precisely drawn around the AL in order to remove from the analysis non-AL regions of the recordings. Finally, the maps obtained for the two to three presentations of each odor were averaged in each individual.

Despite our efforts, individual identification of m-APT glomeruli was not possible. To ensure reliable conclusions, we performed two different types of analyses, a pixelwise analysis on the whole AL surface and a focused analysis on a limited set of glomerular units. For the pixelwise analysis, all pixels of the AL within the mask were used, ensuring a comprehensive and unbiased analysis as it does not depend on any decision made by the experimenter. For intensity measurements, the average of the intensity of all pixels located within the unmasked area was calculated (global activity). To measure similarity relationships between neural activity patterns, the Euclidean distance (a measure of dissimilarity) was calculated pixelwise for all odor pairs within each animal. For the glomerular analysis, the experimenter chose a set of 20 glomerulus-sized areas of interest on each imaged AL, based on activity maps. Each activity spot had a size of 5 × 5 pixels, well within the size of a glomerulus. Activity of all pixels within each spot was averaged. For intensity measurements, the average intensity of all spots was calculated (global activity). To measure similarity relationships, the Euclidean distance was calculated for all odor pairs within each animal, using activity in the 20 spots as main dimensions. Pixelwise and glomerular analyses gave highly correlated values in both subsystems for odor intensity (Pearson correlation $R^2 > 0.79$) and odor similarity measures ($R^2 > 0.74$). Moreover, both analyses yielded exactly the same conclusions concerning coding differences between subsystems. We thus chose to focus on the pixelwise analysis in the text and figures.

To compare similarity relationships among odors at the neural level with data obtained at the behavioral level, we used the Euclidean distances between odors calculated behaviorally by Guerrieri et al. (2005). All results are displayed as means ± SE.

Statistical analysis. Odor-evoked response intensity values were compared with ANOVA for repeated measurements. When significant, Dunnett's test was applied to compare the intensity of each of the 16 odors to a common reference, the air control. In other cases, comparisons of intensity measures among functional groups or chain lengths were done with Tukey post hoc tests.

Wilcoxon matched-pairs tests were applied to compare Euclidean distances between the same and different odors, between odors with the same or with a different functional group, or between odors with the same or with a different chain length. For all analyses, average maps for the three presentations of each odorant were used. One exception was the comparison of Euclidean distances among response maps for the same or different odors (see Fig. 5*A*), which required the use of all individual odor presentations. For this reason, distance values in Fig. 5*A* are not directly comparable with distance values in Fig. 5, *B–D*.

Pearson correlation analyses were performed between response intensity and the logarithm of odorants' vapor pressure and also between physiological and behavioral measures of odor similarity. Mantel tests were used to test whether Pearson correlations between physiological and behavioral measures of odor similarity were significant. All tests were performed with Statistica 5.5 or R (**www.r-project.org**).

RESULTS

Odor-evoked calcium signals from m-APT glomeruli. Calcium imaging was performed after bath application of Calcium

Fig. 1. Calcium signals from glomeruli innervated by the medial antenno-protocerebral tract (m-APT). *A*: schematic drawing of the dual olfactory pathway of the honeybee brain (adapted from Kirschner et al. 2006 with permission). Odorant molecules are detected by olfactory receptor neurons (ORNs) on the antenna, which form the antennal nerve (AN) and send olfactory information to the primary olfactory center, the antennal lobe (AL). Then, projection neurons (PNs) convey information to higher centers, the mushroom bodies (MBs) and the lateral horn (LH), through two main tracts of PNs, the m-APT (pink) and lateral l-APT (green). PNs of the m-APT and l-APT project to distinct areas in the MB and LH. OL, optical lobe. *B*: odor-induced calcium signals in the m-subsystem to a panel of odorants varying according to their carbon chain length (C6–C9) and their chemical functional group (primary and secondary alcohols, aldehydes, and ketones). Relative fluorescence changes (ΔF/F%) are presented in a false-color code, from dark blue to red. Different odors induce different glomerular activity patterns. *C*: anatomical staining (using neutral red) of the inferior part of the AL, using the ventral preparation giving access to the glomeruli of the m-subsystem. A calcium signal to hexanal shown in a false-color code is superimposed on the anatomical image, showing that signals originate from single glomeruli. *D*: typical time course of relative fluorescence changes (ΔF/F%) during a 20-s recording. The presented signal was recorded from *glomerulus C* in response to hexanal (6al), 2-heptanone (2–7one), and the air control. The glomerulus thus responded to hexanal but not to 2-heptanone or air. *E*: calcium responses (ΔF/F%) of 3 example glomeruli on the ventral surface of the AL to the 16-aliphatic odor panel. Functional groups are shown with a color code: primary alcohols in blue, secondary alcohols in green, aldehydes in black, and ketones in red. *Glomerulus A* responds more to short-chain ketones, *glomerulus B* to all ketones, and *glomerulus C* to short-chain aldehydes.

Green-2 AM. Using a novel preparation allowing access to the brain from its ventral side, we could optically record odor-evoked activity from glomeruli innervated by the m-APT PN tract (Fig. 1, *B* and *C*). Together with the traditional preparation used for imaging glomeruli belonging to the l-APT tract (Joerges et al. 1997), both methods allowed us to compare the odor coding properties of the two subsystems. A total of 15 and 16 bees were recorded for the l- and m-subsystems, respectively. Based on counts performed on anatomical afterstaining, the number of potentially imaged glomeruli were 34.6 ± 2.1 glomeruli in the l-subsystem (~41.2% of the 77 glomeruli) and 36.8 ± 1.6 in the m-subsystem (~47.9% of the 84 glomeruli).

The time course of odor-evoked calcium signals in the m-subsystem was the same as that usually obtained in the l-subsystem (Sandoz et al. 2003; Stetter et al. 2001; see above); it was biphasic, with a first positive component followed by a slower negative component and eventually a return to baseline within 20 s (Fig. 1*D*).

Odor quality coding. To explore odor quality coding in both subsystems, we presented 16 aliphatic odorants that differed according to two main chemical features: their functional group (primary and secondary alcohols, aldehydes, and ketones) and the length of their carbon chain (C6, C7, C8, and C9). As found previously for the l-subsystem (Sachse et al. 1999), individual glomeruli in the m-subsystem responded differentially to the panel of odors, as shown for three example glomeruli identified in eight bees (Fig. 1, *C* and *E*). While some glomeruli responded more intensively to particular types of odorants (like short-chain ketones for *glomerulus A* and short-chain aldehydes for *glomerulus C*), others responded to whole functional groups of odorants (*glomerulus B* to ketones). To compare odor coding rules in both subsystems, a global approach was used based on pixelwise analyses of AL activation.

Intensity of AL activity. Odors significantly activated the AL, as they induced significantly higher global activity than air controls, both in the m-subsystems (data not shown; all odorants $P < 0.05$, post hoc Dunnett tests, including a multiple test correction) and in the l-subsystems (15 of 16 odorants, $P < 0.05$, post hoc Dunnett tests).

Different odors produced different levels of activity (odor × subsystem ANOVA, odor effect: $F_{15,195} = 19.2$, $P < 0.001$), and no difference in response intensity was found between the two subsystems [subsystem effect, $F_{1,13} = 2.17$, nonsignificant (NS)]. However, the two subsystems did not respond in the same way to the different odorants, as shown by the significant odor × subsystem interaction ($F_{15,195} = 4.36$, $P < 0.001$).

We thus evaluated how the two subsystems responded as a function of odorant functional group and chain length. Odors with different functional groups activated the AL differently, both in the m-subsystem (Fig. 2*A*, ANOVA $F_{3,21} = 58.35$, $P < 0.001$) and in the l-subsystem (ANOVA $F_{3,18} = 5.39$, $P < 0.01$). More specifically, primary and secondary alcohols induced weaker activation than ketones and aldehydes in the m-subsystem ($P < 0.001$, post hoc Tukey tests). In the l-subsystem, primary alcohols induced weaker activation than all other functional groups ($P < 0.05$, post hoc Tukey tests). Accordingly, the two subsystems were found to respond differentially to the functional groups (subsystem × functional group interaction, $F_{3,39} = 7.92$, $P < 0.001$).

Carbon chain length also affected AL activation, both in the m-subsystem (Fig. 2*B*; ANOVA $F_{3,21} = 8.61$, $P < 0.001$) and in the l-subsystem (ANOVA $F_{3,18} = 39.61$, $P < 0.001$). Thus in the m-subsystem odors with short chain lengths (6 and 7 carbons) induced higher activation than odors composed of 9 carbons (Fig. 2*B*; $P < 0.01$, post hoc Tukey tests). In the l-subsystem, odors with 6 and 7 carbons induced higher neural activity than odors with 8 and 9 carbons (Fig. 2*B*; $P < 0.001$, post hoc Tukey tests). Accordingly, the two subsystems were found to respond differentially to carbon chain lengths (subsystem × chain length ANOVA, interaction, $F_{3,39} = 4.72$, $P < 0.01$).

We then evaluated how well the vapor pressure of an odorant (and therefore its absolute concentration in the stimulus) accounted for AL global response intensity. We found that the more volatile an odorant was the higher was AL neural activity, with a similar and highly significant trend in both subsystems (Fig. 2*C*; m-subsystem: $R^2 = 0.81$, $t = 7.71$, $P < 0.001$; l-subsystem: $R^2 = 0.73$, $t = 6.19$, $P < 0.001$). In particular, alcohols, which have a lower vapor pressure than other functional groups, generally induced weaker AL activation (data not shown). Similarly, odors with short chain lengths, which have a higher vapor pressure than odors with longer chains, induced higher AL activation (data not shown). We thus conclude that at the input to both AL subsystems the intensity of odor-evoked signals is mostly dependent on odorant vapor pressure, even though there are certain biases for particular functional groups and/or carbon chain lengths.

Similarity among odors. To compare qualitative odor coding in both subsystems, we analyzed similarity relationships among response maps for all possible odor pairs ($n = 120$). We thus calculated pixelwise Euclidean distances, obtaining a measure of dissimilarity between any two odor response maps. All analyses were also performed with pixelwise Pearson correlation coefficient among odors, which yielded the same results (data not shown). Figure 3 presents a color-coded matrix of Euclidean distances among odor maps for m- and l-subsystems. Increasing similarity, i.e., decreasing distance, is shown in a color scale from white to red, indicating minimal and maximal similarity, respectively. Similarity within the m-subsystem (Fig. 3, *left*) was highest among alcohols (both primary and secondary), being higher than between alcohols and other functional groups. In the same way, similarity among aldehydes was higher than between aldehydes and other odorants. This influence of functional group on odor-similarity relationships was less clear with ketones. The picture was different in the case of the l-subsystem (Fig. 3, *right*), in which similarity primarily depended on chain length, as shown by the red diagonal lines in the matrix. Thus in the l-subsystem similarity was higher when odors had similar chain lengths, both within functional group (see within primary alcohols or ketones) or between different functional groups (see ketones vs. secondary alcohols). As for functional groups, similarity was highest between primary and secondary alcohols, but also between alcohols and ketones. Aldehydes were highly similar to most other aldehydes but rather different from other odorants.

We confirmed these observations by performing multidimensional analyses using these distance measures (Fig. 4*A*). Cluster analyses (Ward's classification) showed different groupings of odorants in the two subsystems. In the m-subsystem, the analysis separated all alcohols (primary and secondary) from the other odors, which aggregated in two groups representing respectively aldehydes and ketones, with the exception of nonanal, which was grouped with ketones. Primary segregation in the m-subsystem

was therefore based on functional group. Conversely, in the l-subsystem, two of the three main groups depended on chain length. One cluster grouped odors with 6 and 7 carbons, while another cluster grouped odors with 8 and 9 carbons. Aldehydes clearly appeared as a third independent group. Thus, except for aldehydes, the primary segregation criterion in the l-subsystem was carbon chain length.

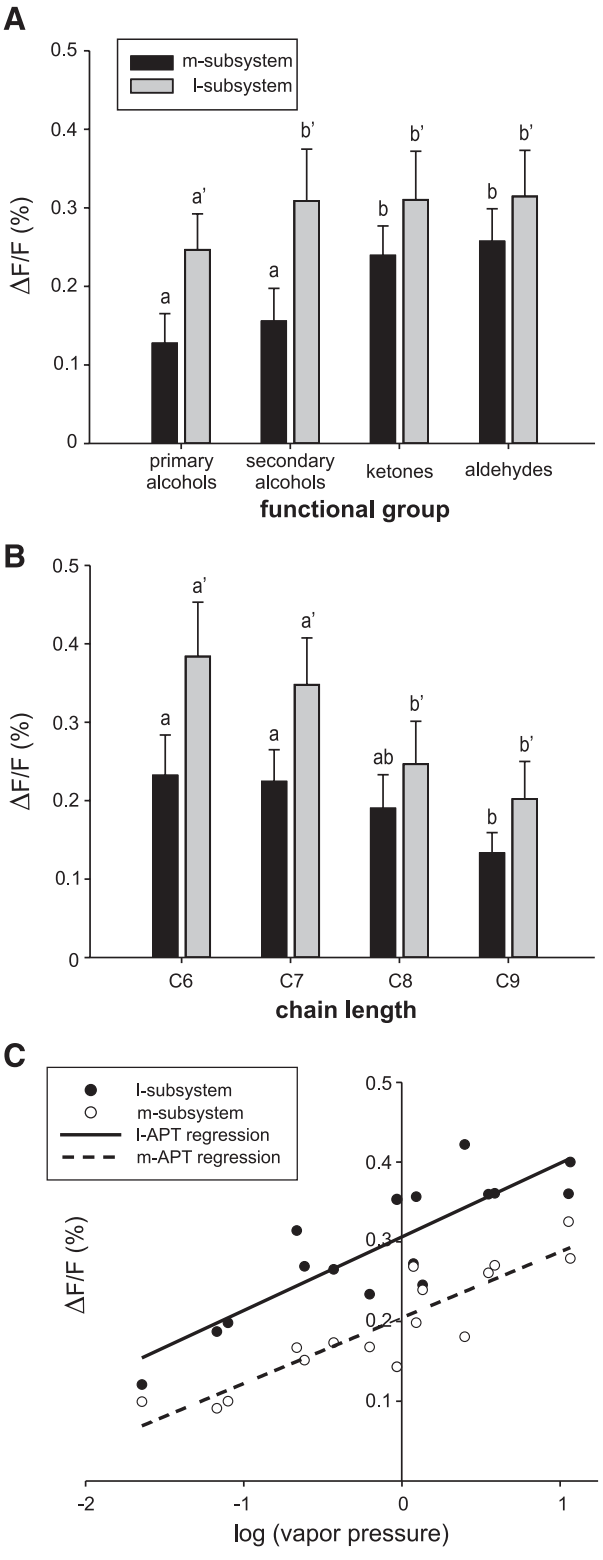

Fig. 2. Odor quality coding: intensity of response to 16 aliphatic odors. *A*: amplitude of calcium responses (ΔF/F%) recorded in both subsystems of the AL (l-APT and m-APT) to different odors according to their functional group (primary and secondary alcohols, aldehydes, and ketones). Primary and secondary alcohols induce weaker activation than aldehydes and ketones in the m-subsystem ($n = 8$; $^{***}P < 0.001$), and, similarly, primary alcohols induce weaker activation than other functional groups in the l-subsystem ($n = 7$; $^{*}P < 0.05$). *B*: amplitude of calcium responses (ΔF/F%) according to odorant carbon chain length (6, 7, 8, and 9 carbons). Odors with the longest carbon chain (C9) induce weaker activation than odors with a short carbon chain (C6 and C7; $^{**}P < 0.01$) in the m-subsystem ($n = 8$). Likewise, odors with a long carbon chain length (C8 and C9) induce higher activation than odors with a short carbon chain length (C8 and C9) in the l-subsystem ($n = 7$; $^{***}P < 0.001$). Error bars indicate SE values across animals. a and b, comparison in the m-subsystem; a′ and b′, comparison in the l-subsystem. *C*: amplitude of calcium responses (ΔF/F%) induced by each of the 16 aliphatic odorants as a function of their vapor pressure. Linear regressions in the m-subsystem ($R^2 = 0.81$, $^{***}P < 0.001$) and in the l-subsystem ($R^2 = 0.73$, $^{***}P < 0.001$) show a significant correlation between the intensity induced by these aliphatic odors and their vapor pressure.

Distance matrices were also used in proximity analyses (also called principal coordinate analyses; Fig. 4*B*), which determine the principal dimensions explaining most of the variance within each data set. Odors are represented as colored arrows (for each functional group) pointing along increasing chain lengths (from C6 to C9). In both cases, three main dimensions allowed explanation of 67.0% and 70.4% of overall variance in the m- and l-subsystems. respectively. In the m-subsystem (Fig. 4*B*, *left*), the first dimension (explaining 34.9% of overall variance) separates alcohols (blue and green arrows) from aldehydes and ketones (black and red arrows, respectively). The second and third dimensions (18.2% and 13.9% of variance) separate ketones and aldehydes, respectively, from other functional groups. The coding of chain length was rather unordered, with most arrows describing complex routes within each plane. We observed in particular that 2-heptanone, an alarm pheromonal compound in bees, was clearly separated from the other ketones (Fig. 4*B*, *left*, *top*). The proximity analysis performed on the l-subsystem (Fig. 4*B*, *right*) defined a first dimension (36.2% of overall variance) that ordered odors based on their carbon chain length (see arrows pointing toward right side of the graph). The second and third dimensions (explaining 23.4% and 10.8% of variance, respectively) separated odors based on functional group. *Dimension 2* segregated aldehydes, alcohols, and ketones. *Dimension 3* separated alcohols from aldehydes and ketones.

To provide statistical evidence for these observations, we compared Euclidean distances between odor response maps. First, to confirm that differences among odor maps correspond to differences in odor coding, we compared Euclidean distances between maps for presentations of the same odor or of different odors. As shown in Fig. 5*A*, odor response maps were more similar (shorter distance) for the same odor than for different odors, both in the m-subsystem (Wilcoxon matched pairs test, $z = 2.52$, $P < 0.05$, 7 df) and the l-subsystem ($z = 2.37$, $P < 0.05$, 6 df). We then compared the Euclidean distances between odor response maps depending upon whether odors presented the same, or a different, functional group or chain length. Odors with the same functional group showed a lower distance, i.e., a higher similarity, than odors with different functional groups (Fig. 5*B*), both in the m-subsystem (Wilcoxon matched pairs test, $z = 2.38$, $P < 0.05$, 7 df) and in the l-subsystem ($z = 2.37$, $P < 0.05$, 6 df). These results indicate that afferences to both the m- and l-subsystems allow

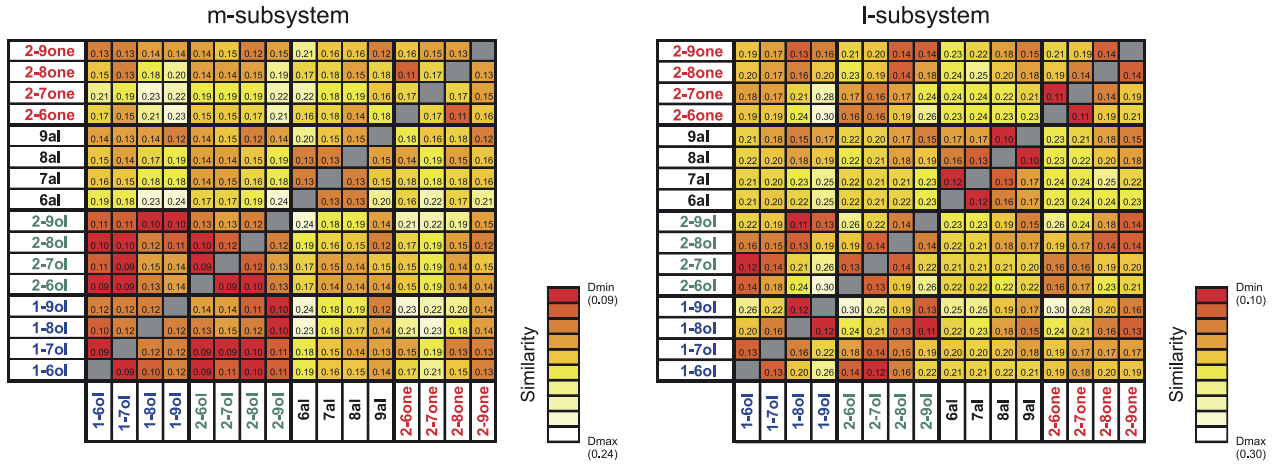

Fig. 3. Odor quality coding: similarity relationships between odors. Similarity among the 16 odors is represented in a false-color matrix, containing the Euclidean distances between the 120 odor pairs, in the m-subsystem (*left*) and the l-subsystem (*right*). Higher similarity (shorter distances, D_{min}) is represented in red, while lower similarity (longer distances, D_{max}) is shown in white. Distances between same odors are represented in gray and correspond to a distance of 0. The m-subsystem matrix shows a functional group coding (principally between alcohols). By contrast, the l-subsystem matrix shows clear chain length coding in the form of diagonal lines of high similarity. This matrix also shows high similarity among aldehydes in comparison to other functional groups.

specific coding of an odorant's functional group. On the other hand, odors with the same carbon chain length were overall as similar as odors with different carbon chain lengths in the m-subsystem (Fig. 5*C*; Wilcoxon matched-pairs test, $z = 0.70$, NS, 7 df). Conversely in the l-subsystem, odors with the same carbon chain length were more similar than odors with different carbon chain lengths (Fig. 5*C*; $z = 2.37$, $P < 0.05$, 6 df). This result indicates that only receptors belonging to the l-subsystem allow for specific coding of carbon chain length. A more detailed representation of odor similarity as a function of chain length coding in both the m- and the l-subsystems is shown in Fig. 5*D*, in which Euclidean distance between any two odors is represented as a function of the difference in their numbers of carbon atoms. Even if the general trend was an increase in distance (decrease in similarity) with increasing carbon chain length difference in both subsystems, this increase was only significant in the l-subsystem (ANOVA $F_{3,18} = 27.9$, $P < 0.001$) and not in the m-subsystem (ANOVA $F_{3,21} = 2.70$, $P = 0.07$). Moreover, a significant interaction was found between carbon chain difference and subsystem (ANOVA $F_{3,39} = 6.61$, $P < 0.005$). This result confirms that the populations of receptors feeding onto the m- and the l-subsystem differ in their properties, as only the l-subsystem efficiently codes chain length information.

These analyses demonstrate that both subsystems receive information about odor quality, but with a clear difference. The m-subsystem receives mostly information about an odorant's functional group, whereas the l-subsystem receives information about both carbon chain length and functional group.

Correlation between optophysiological and behavioral measures of odor similarity. We then asked how efficiently optophysiological measures of odor similarity recorded in the two subsystems allow prediction of perceptual relationships among odors when measured behaviorally. A previous study provided a matrix of perceptual similarity among these 16 odorants, based on the generalization responses of bees in an appetitive conditioning experiment (Guerrieri et al. 2005). We thus performed correlation analyses between Euclidean distances among the 120 odor pairs obtained in imaging and in behavior, separately for m- and l-subsystems (Fig. 6, *A* and *B*). Neurophysiological and behavioral distances were significantly correlated both in the m-subsystem (Fig. 6*A*; Mantel test $R^2 = 0.13$, $P < 0.002$) and in the l-subsystem (Fig. 6*B*; Mantel test, $R^2 = 0.55$, $P < 0.001$). This result shows that odors evoking similar activity patterns in either of the two subsystems are treated as similar by honeybees in their behavior. However, the similarity measures recorded in the l-subsystem allowed a better prediction of olfactory perception than measures taken in the m-subsystem (R homogeneity test, $P < 0.002$).

We then asked within each subsystem which characteristics of odor molecules, i.e., functional group or chain length, yield the best correlation between behavioral and neurophysiological data. We thus performed these correlations by taking into

Fig. 4. Odor quality coding: cluster and proximity analyses of similarity measures. *A*: cluster analysis showing similarity relationships among odors in both AL subsystems (using Ward's classification method). *Left*: m-subsystem ($n = 8$). *Right*: l-subsystem ($n = 7$). The higher the linkage distance the more dissimilar odors are. In both analyses, functional groups are shown with a color code: primary alcohols in blue, secondary alcohols in green, aldehydes in black, and ketones in red. The dendrogram on the m-subsystem (*left*) clearly shows a separation between all alcohols and other odors. Within these classes, alcohols with short chain lengths are separated from alcohols with long chain lengths, and aldehydes are mostly separated from ketones. The same cluster analysis performed on the l-subsystem (*right*) shows a primary separation between odors with short chain lengths (6 and 7 carbons) and odors with long chain lengths (8 and 9 carbons), except for aldehydes, which form a clearly isolated group. *B*: proximity analysis using Euclidean distances obtained for the 120 odor pairs in the m- and l-subsystems. For the m-subsystem (*top left*) the first dimension explains 34.9% of the variance and separates alcohols (blue and green) from aldehydes and ketones (black and red). The second dimension explains 18.2% of the variance and separates ketones (red) from other functional groups. The third dimension (*bottom left*) explains 13.9% of the variance and allows the separation of aldehydes (black) from other odors. Chain length (see C6–C9 labels and arrow) is not clearly represented by any dimension in the m-subsystem. Proximity analysis on the l-subsystem defines a first dimension (*top right*) explaining 36.2% of the variance, which separates odors depending on their carbon chain length (all arrows point to *right*). The second dimension explains 23.4% of the variance and allows the separation of aldehydes (black) from other functional groups. The third (*bottom right*) explains 10.8% of the variance and separates alcohols (blue and green) from aldehydes and ketones (black and red). Chain length and also functional group are represented in the l-subsystem.

account functional group and chain length information separately (Fig. 6, *C* and *D*). To evaluate the information content corresponding to the functional group, we kept odor pairs that differed in their functional group but not in their chain length ($n = 24$; for instance, 1-hexanol vs. 2-hexanone). Conversely, for evaluating information content corresponding to chain length, we kept odor pairs that differed in their chain length but had the same functional group ($n = 24$; for instance, heptanal vs. nonanal). In the m-subsystem, pattern distances could only predict behavioral responses when functional group informa-

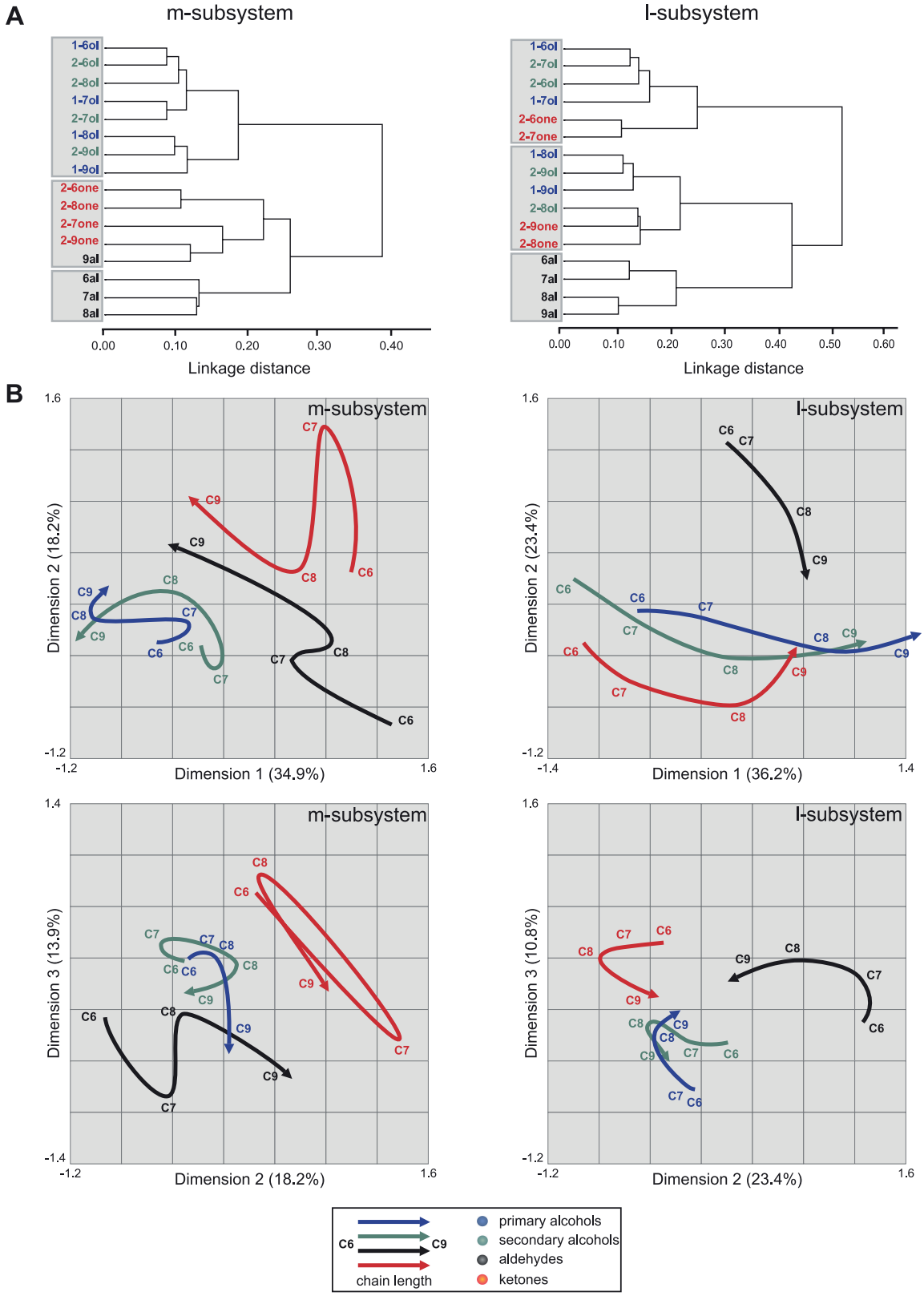

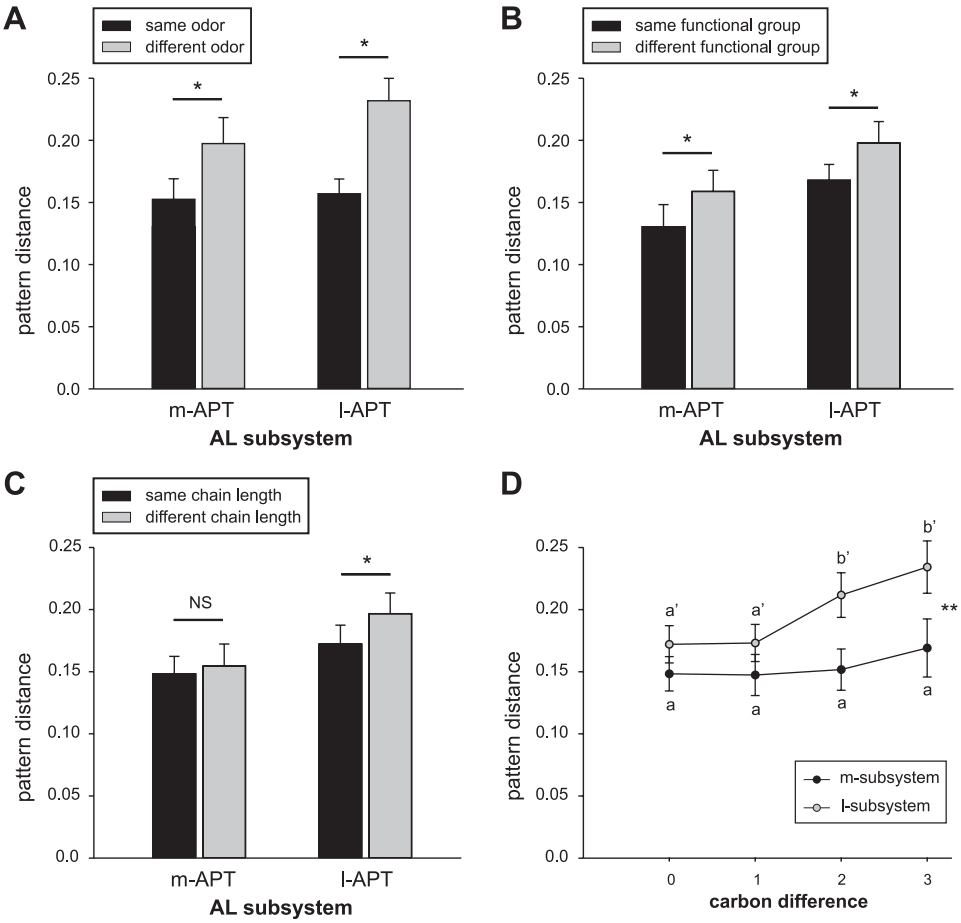

Fig. 5. Odor quality coding: similarity depending on functional group or carbon chain length. *A*: similarity between presentations of the same odor or of different odors in both AL subsystems. Activity maps are more similar when the same odor is presented, showing specific odor coding in both subsystems ($^*P < 0.05$). *B*: similarity between odors with the same or different functional groups. Odors with the same functional group induce more similar glomerular activity patterns than odors with different functional groups in both subsystems ($^*P < 0.05$). *C*: similarity between odors with the same or different carbon chain lengths in both AL subsystems of the AL. Odors with the same chain length induce more similar glomerular activity patterns than odors with different chain lengths in the l-subsystem ($^*P < 0.05$), whereas in the m-subsystem activity patterns are as similar between odors with the same and with a different chain length (NS, nonsignificant). *D*: similarity between odors depending on the difference in their number of carbon atoms, for both m- and l-subsystems. The general trend is an increase of Euclidean distance with increasing difference in the number of carbons in both subsystems, but it is only significant in the l-subsystem ($^{**}P < 0.01$). a, comparison in the m-subsystem; a′ and b′, comparison in the l-subsystem.

tion (Fig. 6*C*, *left*; $R^2 = 0.33$, $P < 0.01$) but not chain length information (Fig. 6*C*, *right*; $R^2 = 0.01$, NS) was considered. By contrast, in the l-subsystem, both functional group and chain length information accounted well for the behavioral data ($R^2 = 0.60$ in both cases, $P < 0.001$).

These results show that the m-subsystem receives information about an odorant's functional group, which allows prediction of bees' behavior, but information about an odorant's chain length is not necessarily conveyed. The l-subsystem receives information about both functional group and chain length, both of which can separately predict bees' behavior.

Odor quantity coding. We then focused on the effect of odor concentration on olfactory coding in both olfactory subsystems. We chose three odorants (1-hexanol, heptanal, and 2-octanone), which were well differentiated by both subsystems in the previous experiment, and recorded calcium responses triggered by these odors at eight concentrations ranging from 10^{-7} to 10^{0}. Increasing concentrations of an odorant (here 2-octanone) led to increasing global activity in both m- and l-subsystems, with more glomeruli entering the activity pattern at higher concentrations (Fig. 7*A*). As shown previously for glomeruli in the l-subsystem (Sachse and Galizia 2003), glomeruli in the m-subsystem responded in a dose-dependent manner. For the example glomeruli presented in Fig. 1*C*, *glomeruli A* and *B* showed increasing responses to 2-octanone, and to a lesser extent to heptanal and 1-hexanol (Fig. 7*B*). On the other hand, *glomerulus C* showed a similar dose-response relationship for heptanal and 2-octanone and lower responses to 1-hexanol. Odor responses were usually visible starting at 10^{-3} or 10^{-2} concentrations.

To compare dose-response relationships between the AL subsystems, global response amplitudes (averaging activity from all pixels on the AL surface) were normalized to maximum intensity within each honeybee (usually obtained for 10^{-1} or 10^{0} concentration) and dose-response curves were calculated for the three tested odors by averaging across animals (Fig. 7*C*; $n = 8$ in both subsystems). A similar dose-response relationship was found in the m-subsystem and in the l-subsystem. All three odors displayed a significant increase in neural activity with increasing concentrations in both subsystems (m-subsystem: $F_{7,49} > 8.57$, $P < 0.001$; l-subsystem: $F_{7,49} > 15.74$, $P < 0.001$). Comparison of dose-response curves in the two subsystems shows that responses to 1-hexanol and to heptanal were generally higher in the l-subsystem than in the m-subsystem (subsystem × concentration ANOVA, subsystem effect, $F_{1,14} = 5.65$, $P < 0.05$ and $F_{1,14} = 9.15$, $P < 0.01$, respectively). This was not the case for 2-octanone ($F_{1,14} = 1.93$, NS). However, responses to all three odors followed a similar dose-response curve in the two subsystems, as none of the interactions between concentration and subsystem was significant (subsystem × concentration interaction, $F_{7,98} < 1.44$ for the 3 odors, NS). Indeed, the first concentrations at which response to each odorant was significantly different from the control (mineral oil) were 10^{-2} for 1-hexanol in both subsystems, 10^{-2} for heptanal in both subsystems, and 10^{-3} and 10^{-2} for 2-octanone in the m- and

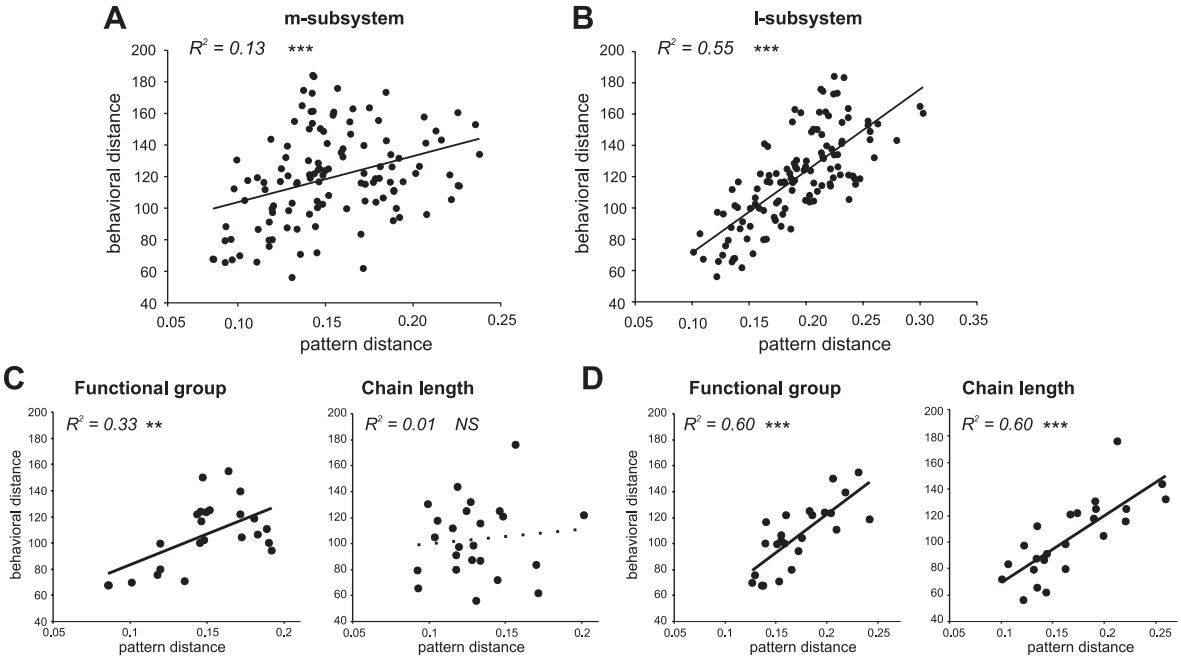

Fig. 6. Odor quality coding: relationship between perceptual and physiological odor similarity measures. *A*: correlation of distances between odors obtained from optophysiological measurements in the m-subsystem (calcium imaging recordings) and behavioral experiments (Guerrieri et al. 2005). A slight but significant correlation is observed for the 120 odor pairs studied ($R^2 = 0.13$, $^{***}P < 0.001$). *B*: similar correlation between distances obtained from optophysiological measures in the l-subsystem and behavioral measures (Guerrieri et al. 2005). A high and significant correlation is observed for the same 120 odor pairs ($R^2 = 0.55$, $^{***}P < 0.001$). *C*: correlation between optophysiological measures in the m-subsystem and behavioral measures (Guerrieri et al. 2005) depending on odorants' functional group (*left*) and carbon chain length (*right*). In the m-subsystem, distances are correlated depending on functional group ($R^2 = 0.33$, $^{**}P < 0.01$) but not depending on chain length ($R^2 = 0.01$, NS). *D*: correlation between optophysiological measures in the l-subsystem and behavioral measures (Guerrieri et al. 2005) depending on odorant functional group (*left*) and carbon chain length (*right*). In the l-subsystem, distances are highly correlated depending on both functional group ($R^2 = 0.60$, $^{***}P < 0.001$) and carbon chain length ($R^2 = 0.60$, $^{***}P < 0.001$).

l-subsystems, respectively (post hoc Dunnett tests, $P < 0.05$). Thus higher concentrations of these odorants were considered as belonging to the "coding" domain (see below).

Similarity among odors as a function of concentration. We analyzed how similarity between odors was affected by odorant concentration in both subsystems. Euclidean distances between response maps for all ($n = 276$) pairs of stimuli were calculated as above. Cluster analyses yielded a very similar classification in both subsystems (Fig. 8*A*). The main separation was mostly between concentrations that yielded a clear and significant signal ("coding" in Fig. 8*A*; see above) and concentrations that gave a signal close to baseline activity ("baseline" in Fig. 8*A*). In both subsystems, the same three concentrations (from 10^{-2} to 10^{0}) of each odorant were classified in the "coding" cluster. *Subclusters 2* and *3* were formed by heptanal and 2-octanone, each odor at their two highest concentrations, in both subsystems. Another subcluster, *subcluster 1*, included all concentrations of 1-hexanol and the 10^{-2} concentrations of heptanal and 2-octanone. These observations are confirmed by proximity analyses extracting three main dimensions explaining 80.8% and 83.2% of overall variance in the m- and l-subsystems, respectively. In Fig. 8*B*, odors are represented as colored arrows (for each odor) pointing along increasing concentrations (from 10^{-7} to 10^{0}). Odor repartition was very similar in both subsystems, with a first dimension taking into account signal intensity thus closely following odor concentration (from *left* to *right* in Fig. 8*B*). A second factor allowed clear differentiation between heptanal and 2-octanone in both subsystems and provided some separation of 1-hexanol from the two other odors in the l-subsystem but not in the m-subsystem. However, this separation was clearly achieved by the third dimension in both subsystems. Thus qualitative relationships between the three odors at different concentrations were nearly identical in both subsystems.

We then asked how similarity among odors evolved with increasing concentrations of the three odors. Figure 9 presents the average distance between activity patterns of all three odors presented at the same concentration, from 10^{-7} to 10^{0}. As expected, distances between odors increased with increasing concentration, so that the similarity between odors decreased. This effect was clear both in the m-subsystem (Fig. 9, *left*; odor pair × concentration ANOVA, $F_{7,147} = 28.84$, $P < 0.001$) and in the l-subsystem (Fig. 9, *right*; odor pair × concentration ANOVA, $F_{7,147} = 31.69$, $P < 0.001$). The evolution of odor similarity relationships with increasing concentrations was similar in both subsystems, as no interaction was found between concentration and subsystem (odor pair × concentration × subsystem ANOVA, concentration × subsystem interaction, $F_{7,98} = 0.49$, NS). We conclude from these observations that receptor neurons conveying olfactory information to both AL subsystems encode odors at different concentrations in a very similar way.

DISCUSSION

We successfully recorded activity from receptor afferences that convey olfactory information to glomeruli innervated by m-APT and l-APT PNs in the honeybee AL. The novelty of our procedure consisted in the fact that we were able to record activity maps in the m-APT subsystem, whose glomeruli have

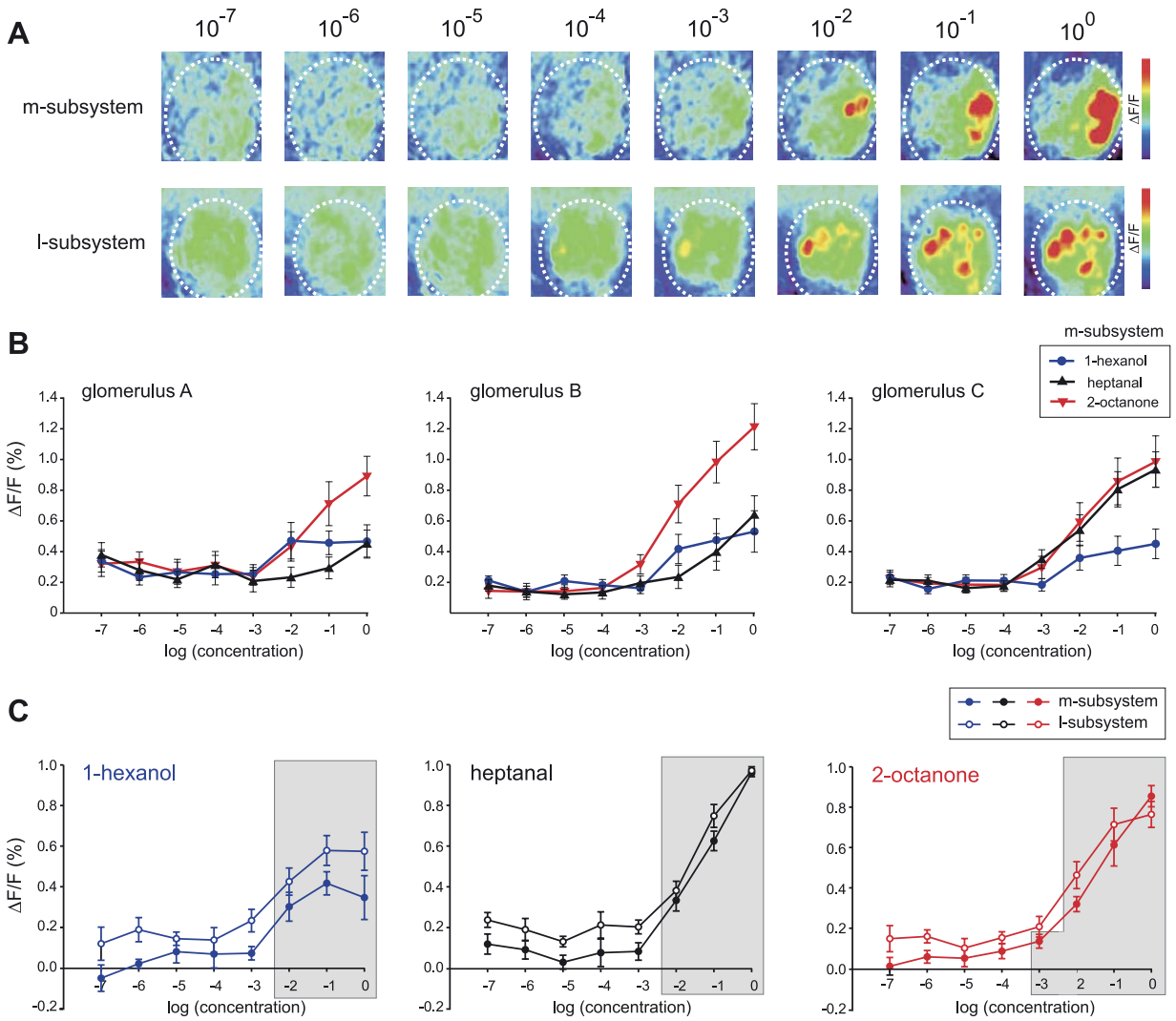

Fig. 7. Odor quantity coding: odor-induced intensity with increasing concentration. *A*: activity maps of odor-induced calcium signals with increasing concentrations of 2-octanone in the m (*top*)- and l (*bottom*)-subsystems. Relative fluorescence changes (ΔF/F%) are presented in a false color code, from dark blue to red. Increasing concentrations lead to an increase in signal amplitude and an increase in the number of activated glomeruli, in a similar manner in both subsystems of the AL. *B*: dose-response curves to 3 odorants at 8 concentrations in the 3 identified m-subsystem glomeruli presented in Fig. 1*C*. Increasing odor concentrations lead to increased neural activity in all 3 glomeruli, with different odor specificities for each glomerulus. *C*: dose-response curves for 3 odorants are shown after normalization to the strongest odor response within each animal: relative fluorescence changes (ΔF/F%) depending on concentration for 1-hexanol (*left*), heptanal (*middle*), and 2-octanone (*right*). Dose-response curves show that increasing odor concentrations lead to an increase in neural activity, both in the m-subsystem (for all odors $***P < 0.001$) and in the l-subsystem (for all odors $***P < 0.001$). In the 3 dose-response curves, concentrations of each odorant that induce a signal significantly higher than the air control are represented in a gray box. Dose-response curves were not significantly different between the 2 AL subsystems.

remained inaccessible until now given their hidden location on the posterior side of the AL. These glomeruli responded to the whole range of tested aliphatic odorants, allowing direct comparison of olfactory coding at the AL input level between the m- and l-subsystems. Our results show that each subsystem harbors different properties of odor quality coding, as m-subsystem receptors mostly inform the AL about an odor's functional group while l-subsystem receptors provide most strongly chain length information while also retaining functional group information. Accordingly, both subsystems can significantly predict perceptual relationships among odors as measured behaviorally. Finally, each subsystem shows similar responses as a function of odor concentration.

Odor quality coding. The main difficulty we faced in the present study was glomerulus identification in the m-subsystem. A reference atlas of the honeybee AL (Galizia et al. 1999a) has been used effectively, including by us, for recognizing a set of ~20 glomeruli in the l-subsystem, which have typical shapes, sizes, and conserved relative positions (e.g., Deisig et al. 2006, 2010; Fernandez et al. 2009; Galizia et al. 1999b, Hourcade et al. 2009; Sachse et al. 1999). For the glomeruli of the m-subsystem, which are much more similar in shape and size, such irrefutable systematic identification was not possible. Even if we managed to recognize a few such glomeruli between individuals (see *glomeruli A–C*, Figs. 1*E* and 7*B*), this was not possible for many m-APT glomeruli. Thus, to compare odor coding rules in an equivalent manner in both subsystems, we chose a pixel-based approach, which does not rely on any identification by the experimenter. This approach proved to be successful, as our results for the l-subsys-

tem fully confirmed and extended those obtained by Sachse et al. (1999), who recorded glomerular responses from identified glomeruli in the ventral part of the AL, innervated by l-APT neurons. We found similar variation of global response intensity as a function of chain length and functional groups (Fig. 2) and coincident similarity relationships among odorants (Figs. 3 and 4) and confirmed the ability of l-subsystem activity maps to efficiently predict behavioral data (comparison with Guerrieri et al. 2005; Fig. 6). These facts validate our pixel-based analysis of odor response maps in the AL and allow direct comparison of odor coding rules between m- and l-subsystems. As an additional confirmation, we performed all analyses with a set of 20 areas of interest in each imaged AL and confirmed all the results presented here with the pixelwise analysis (see MATERIALS AND METHODS), thus showing that our conclusions do not depend on the method chosen for quantifying neural activity. We are therefore confident that the approach chosen to measure and compare odor-evoked activity between subsystems was pertinent.

In both subsystems, response intensity depended on an odor's functional group and chain length. Although subtle differences were observed between subsystems (for instance, secondary alcohols induced more activity relative to other odorants in the l- than in the m-subsystem; Fig. 2*A*), the same general relationships were found in both subsystems (Fig. 2*A*). Thus odors carrying a carbonyl group (C=O), like ketones and aldehydes, activate the AL more strongly than odors carrying a hydroxyl (C-OH) group, like alcohols (Fig. 2*A*). Moreover, activity generally decreased with increasing chain length (Fig. 2*B*). Indeed, as found by Sachse et al. (1999), the correlation between odorants' vapor pressure and AL activity was very strong. We show that this relationship is similar in both subsystems (Fig. 2*C*). We thus conclude that olfactory receptors conveying information to the l- and m-subsystems respond in a similar and rather unbiased manner to aliphatic odors, so that AL activity mainly reflects odor concentration in vapor phase. This conclusion is confirmed by our recordings with increasing odor concentrations, in which very similar dose-response relationships were obtained for three odors at eight different concentrations (Fig. 7).

Despite these coincident features, similarity relationships among odorants were different between m- and l-subsystems. The use of multidimensional analyses (Fig. 4) showed that while the m-subsystem receptors respond to odorants primarily based on their functional group, l-subsystem receptors principally respond to odors according to their chain length. This last result confirms previous work in which carbon chain length was the main variable influencing glomerular response profiles in the l-subsystem (Sachse et al. 1999). The apparent segregation of olfactory information between subsystems is only partial, however, as a good degree of functional group coding can be found in the l-subsystem (Figs. 4*B* and 5*B*). In the m-subsystem, although the effect of chain length was not significant when measured on a difference of four carbons in the aliphatic chain, a general trend was observed that may be significant when comparing wider differences in the carbon numbers (Fig. 5*D*). Thus chain length coding may also exist in the m-subsystem.

The respective specificities of each subsystem for odor quality coding were confirmed when we attempted to predict perceptual relationships among odors, which were measured behaviorally in a previous work (Guerrieri et al. 2005). Calcium activity signals obtained in both subsystems correlated significantly with the behavioral data, but signals from the l-subsystem allowed a better prediction than those of the m-subsystem (Fig. 6, *A* and *B*). This result can be explained by the fact that the generalization behavior of bees with these 16 odorants varied depending both on functional group and on carbon chain length (Guerrieri et al. 2005). Indeed, the putative olfactory space that was extracted from the behavioral data had functional group and carbon chain length as inner dimensions. Thus a subsystem that codes these two features (the l-subsystem) was logically better at predicting the behavioral data than a subsystem strongly biased toward one of these features (the m-subsystem).

This principle of neural mapping depending on functional group and carbon chain length is a general finding in the animal kingdom, from the insect AL (Couto et al. 2005; Dupuy et al. 2010; Hansson et al. 2003; Lei et al. 2004; Wang et al. 2003) to the vertebrate olfactory bulb (Johnson and Leon 2007; Mori et al. 2006). In the olfactory bulb, odor coding is organized chemotopically according to two classes of features: primary features (functional groups) that characterize whole glomerular domains (whole bulbar regions; Igarashi and Mori 2005; Takahashi et al. 2004; Uchida et al. 2000) and secondary features (carbon chain length and branching) that are represented by local positions within each domain (Johnson and Leon 2000b, 2004; Rubin and Katz 1999; Uchida et al. 2000). Thus, in rats, functional group would be the main feature differentiating aliphatic odors, while carbon chain length would rather represent a secondary feature. This conclusion seems also to be supported by perceptual experiments in humans, in which functional groups strongly influence odor quality while carbon chain length and branching have a relatively minor influence on odor quality (Beets 1970; Laska and Teubner 1999; Nagao et al. 2002; Polak 1973). Accordingly, in honeybees functional group information would be provided by both subsystems, while chain length information would be specifically provided by only one subsystem. Our data thus provide the first clue based on a rather wide and identical odorant panel that two classes of olfactory receptors feeding on the l- and m-olfactory subsystems of the honeybee may code odor features differentially.

Odor quantity coding. Honeybees show high behavioral generalization between concentrations of the same odorant (Bhagavan and Smith 1997; Getz and Smith 1991; Marfaing et al. 1989; Pelz et al. 1997). At the same time, they seem to be able to differentiate between two concentrations of the same odor if the intensity differs by at least a factor of 100 (Ditzen et al. 2003; Getz and Smith 1991; Kramer 1976; but see Pelz et al. 1997). These behavioral studies suggest the existence of both concentration-specific coding and a certain level of concentration invariance of odor coding. Our recordings found similar dose-response curves and interodor similarity relationships in l- and m-subsystems. As observed by Sachse and Galizia (2003) for the l-subsystem, increasing odor concentration resulted in more activated glomeruli (i.e., more activated pixels in our study). Such gradual recruitment of glomeruli with increasing odor concentration is a common observation in vertebrates (Friedrich and Korsching 1997; Meister and Bonhoeffer 2001; Rubin and Katz 1999) and invertebrates (Ng et al. 2002; Wang et al. 2003). It can easily be explained by the gradual activation of more ORNs for which the odorant is only a secondary ligand (de Bruyne et al. 2001; Duchamp-Viret et al.

2000; Hallem and Carlsson 2006; Vareschi 1971). Thus odor coding in both l- and m-subsystems was highly overlapping between concentrations of the same odorant but also showed topical differences, with secondary glomeruli in the pattern missing at lower concentrations. However, the basis for the separation between concentration invariance and concentration dependence may be found downstream of the olfactory pathway. A recent study compared the calcium responses of m-APT and l-APT PN boutons in the MB calyces (Yamagata et al. 2009). Responses of l-APT boutons were clearly less concentration dependent than those of m-APT boutons, an effect that was not found in our recordings at the level of the input to AL glomeruli. Similarly, Sachse and Galizia (2003) noted a strong concentration dependence on the dendritic side of l-APT PNs in the AL. Therefore, the

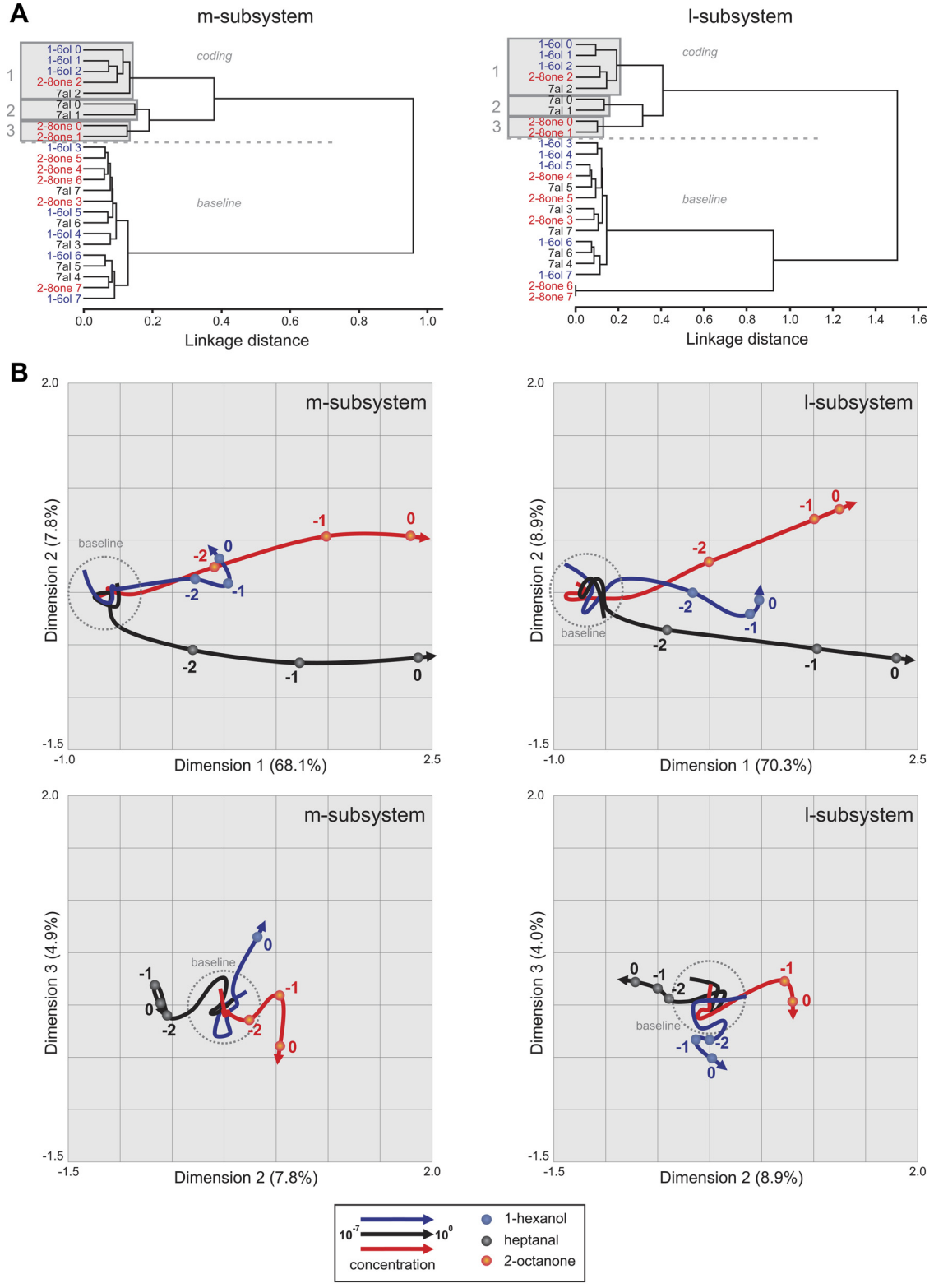

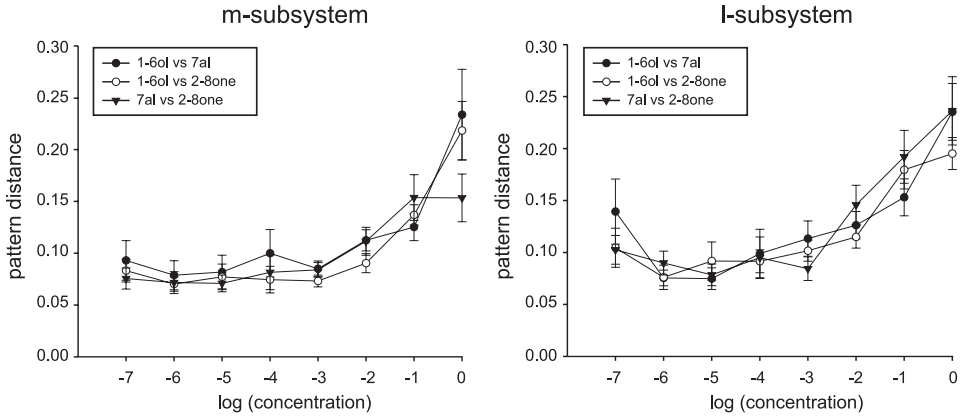

Fig. 9. Odor quantity coding: pattern distances depending on odor concentration. Distances between odor-evoked patterns at each concentration (1-hexanol vs. heptanal, 1-hexanol vs. 2-octanone, and heptanal vs. 2-octanone), depending on the concentration (log). The distances between odors increase with increasing concentrations in the m-subsystem (*left*; $***P < 0.001$) as well as in the l-subsystem (*right*; $***P < 0.001$).

current interpretation of the data by Yamagata et al. (2009) is that the relative loss of concentration dependence within the l-subsystem could be due to presynaptic gain control by a global inhibition system at the level of the calyx lip (see also Schmuker et al. 2011). GABAergic feedback neurons (also called PCT neurons) are known to provide recurrent inhibition to olfactory microglomeruli in the calyx and to be activated by odors (Ganeshina and Menzel 2001; Grünewald 1999; Haehnel and Menzel 2010). Since our work shows that l- and m- subsystems support the same dose-response relationships in the AL, it suggests that the weight of inhibitory input may be different between l- and m-APT boutons, so that gain control would predominantly affect l-APT boutons. Such differential gain control on the two subsystems may represent a mechanism for providing both a concentration-invariant coding in the l-subsystem and a strongly concentration-dependent coding in the m-subsystem.

Odor detection repertoire. We bath applied a permeable calcium-sensitive dye, Calcium Green-2 AM, on the brain before recording odor-evoked activity. With this protocol, all AL cells could potentially be stained (ORNs, PNs, local inhibitory interneurons, glia) but the recorded signals are mainly related to ORN input (Deisig et al. 2010; Galizia et al. 1998; Sachse et al. 2003). Following the current hypothesis that each glomerulus is the projection center for ORNs expressing a particular odorant receptor (OR) (Couto et al. 2005; Kreher et al. 2005; Vosshall et al. 2000), the physical arrangement of the glomeruli at the AL surface can be viewed as a sensory array representing the ~163 types of functional ORs known in the bee (Robertson and Wanner 2006). Therefore, the glomeruli of l- and m-subsystems may represent two nonoverlapping sets of ORs, that is, two independent portions of the honeybee odor detection repertoire. ORs come in a wide array of tuning breadth and response spectra, and often respond to general molecular features such as functional group or carbon chain length in vertebrates (Araneda et al. 2000; Malnic et al. 1999; Zhao et al. 1998) as well as in invertebrates (Couto et al. 2005; Hallem and Carlson 2006). It can thus be speculated that ORs belonging to the l- and m-subsystems would have differing sensitivity spectra, with ORs of the m-subsystem being generally more specific for particular functional groups than for chain lengths and ORs of the l-subsystem being more specific for particular chain lengths than for functional groups. In *Drosophila*, the physical distance between any two AL glomeruli is correlated with the genomic sequence difference between ORs expressed in the ORNs targeting these glomeruli (Couto et al. 2005). Following this observation, one may imagine that ORs belonging to two clearly segregated subsystems actually form two phylogenetically different subgroups of ORs in the honeybee genome. Observation of cladiograms of honeybee ORs (Fig. 1 in Robertson and Wanner 2006) suggests that among the 157 ORs belonging to the honeybee-specific expansion, a major separation gives rise to two main subgroups of ~75 ORs. To progress in our understanding of the evolutionary origin of this olfactory system based on two subsystems of equivalent size, a specificity of Hymenoptera among insects (Galizia and Rössler 2010), a careful mapping of ORs onto identified glomeruli will be necessary.

Future prospects. Thanks to our novel preparation, it is now possible to access both l- and m-subsystems optically and to record activity from a substantial and equivalent portion of both subsystems (>40% of the glomeruli in both subsystems). It should be kept in mind that the nonimaged glomeruli could provide additional properties to each subsystem, such as, for instance, a chain length dependence in the m-subsystem. Coupling our preparation with additional techniques like gold mirrors (Galizia et al. 2012) or two-photon microscopy (Brandstaetter and Kleineidam 2011) may allow access to a more important part of both subsystems. Concerning odor coding,

Fig. 8. Odor quantity coding: cluster and proximity analyses on similarity measures. *A*: cluster analysis showing similarity relationships among odors at different concentrations in both AL subsystems (using Ward's classification method). *Left*: m-subsystem ($n = 8$). *Right*: l-subsystem ($n = 7$). Different odors are shown with different color codes, and the last digit indicates the concentration (4 represents the 10^{-4} concentration). The dendrogram for the m-subsystem (*left*) clearly shows a separation between high concentrations (10^{0} to 10^{-2} coding part in gray) and weak concentrations (10^{-3} to 10^{-7}, baseline) of all odors. The same analysis for the l-subsystem (*right*) shows exactly the same separation, with the same sorting of high concentration odors. *B*: proximity analysis using the 276 Euclidean distances arising from the 3 odors at 8 concentrations for the m-subsystem (*left*) and the l-subsystem (*right*). Small labels indicate odorant concentrations that are statistically different from the control ("coding," see Fig. 7*C*). Arrows point toward increasing concentrations. In the m-subsystem, the analysis defines a first dimension (*top left*) explaining 68.1% of the variance, which separates odors depending on their concentration (arrows pointing to *right*). The second dimension explains 7.8% of the variance and separates mostly heptanal from 2-octanone and 1-hexanol. The third dimension (*bottom left*) explains 4.9% of the variance and allows the separation of 1-hexanol from other odors. The proximity analysis performed on the l-subsystem yields essentially the same results: it defines a first dimension (*top right*) explaining 70.3% of the variance, which separates odors depending on their concentration (all arrows point to *right*). The second and third dimensions explaining 8.9% and 4.0% of the variance respectively, allow the separation of the different odors.

we have shown that l- and m-subsystems respond differentially to chain length and functional group, two major features of olfactory molecules influencing odor quality. However, many other features remain to be tested, such as cyclization, bond saturation, or branching (Johnson and Leon 2000a, 2000b, 2004, 2007). Moreover, as honeybees rely on a range of social pheromones for the organization and maintenance of the colony (Free 1987; Sandoz et al. 2007), future work should evaluate whether and how these pheromones are represented in the m-subsystem compared with the l-subsystem. Finally, combining this preparation with specific staining of PNs of the m-APT tract will allow progress in our understanding of the commonalities versus specificities of olfactory processing in the m-subsystem relative to the l-subsystem, especially regarding the transformation of the olfactory message in the AL due to lateral inhibition (Deisig et al. 2010; Krofczik et al. 2009; Sachse and Galizia 2003; Yamagata et al. 2009).

ACKNOWLEDGMENTS

We thank Maud Combe for developing the custom programs used for data analysis and Gabriela de Brito Sanchez for helping with the development of the m-APT imaging preparation. We are also thankful to Dr. Ch. Kleineidam for helpful discussions.

GRANTS

We thank the ANR (Project EVOLBEE, 2010-BLAN-1712-01 to J.-C. Sandoz), the French Research Ministry (J. Carcaud), and the ERASMUS program (T. Hill). We also thank the French National Research Council (CNRS) and the University Paul Sabatier (Program APIGENE) for support.

DISCLOSURES

No conflicts of interest, financial or otherwise, are declared by the author(s).

AUTHOR CONTRIBUTIONS

Author contributions: J.C., M.G., and J.-C.S. conception and design of research; J.C. and T.H. performed experiments; J.C. and J.-C.S. analyzed data; J.C., M.G., and J.-C.S. interpreted results of experiments; J.C. and J.-C.S. prepared figures; J.C. and J.-C.S. drafted manuscript; J.C., M.G., and J.-C.S. edited and revised manuscript; J.C., T.H., M.G., and J.-C.S. approved final version of manuscript.

REFERENCES

Abel R, Rybak J, Fietz A, Menzel R. Structure and response patterns of olfactory interneurons in the honeybee, *Apis mellifera*. *J Comp Neurol* 437: 363–383, 2001.

Alcock J. *Animal Behavior, an Evolutionary Approach*(6th ed.). Sunderland, MA: Sinauer, 1998.

Araneda RC, Kini AD, Firestein S. The molecular receptive range of an odorant receptor. *Nat Neurosci* 3: 1248–1255, 2000.

Asahina K, Louis M, Piccinotti S, Vosshall LB. A circuit supporting concentration-invariant odor perception in *Drosophila*. *J Biol* 8: 9, 2009.

Bhagavan S, Smith BH. Olfactory conditioning in the honey bee, *Apis mellifera*: effects of odor intensity. *Physiol Behav* 61: 107–117, 1997.

Beets MG. The molecular parameters of olfactory response. *Pharmacol Rev* 22: 1–34, 1970.

Brandstaetter AS, Kleineidam CJ. Distributed representation of social odors indicates parallel processing in the antennal lobe of ants. *J Neurophysiol* 106: 2437–2449, 2011.

Couto A, Alenius M, Dickson BJ. Molecular, anatomical, and functional organization of the *Drosophila* olfactory system. *Curr Biol* 15: 1535–1547, 2005.

Datta SR, Vasconcelos ML, Ruta V, Luo S, Wong A, Demir E, Flores J, Balonze K, Dickson BJ, Axel R. The *Drosophila* pheromone cVA activates a sexually dimorphic neural circuit. *Nature* 452: 473–477, 2008.

de Bruyne M, Foster K, Carlson JR. Odor coding in the *Drosophila* antenna. *Neuron* 30: 537–552, 2001.

Deisig N, Giurfa M, Lachnit H, Sandoz JC. Neural representation of olfactory mixtures in the honeybee antennal lobe. *Eur J Neurosci* 24: 1161–1174, 2006.

Deisig N, Giurfa M, Sandoz JC. Improved discriminability of odor mixture representation at the level of projection neurons in the honeybee antennal lobe. *J Neurophysiol* 103: 2185–2194, 2010.

Derby CD. Learning from spiny lobsters about chemosensory coding of mixtures. *Physiol Behav* 69: 203–209, 2000.

Ditzen M, Evers JF, Galizia CG. Odor similarity does not influence the time needed for odor processing. *Chem Senses* 28: 781–789, 2003.

Duchamp-Viret P, Duchamp A, Chaput MA. Peripheral odor coding in the rat and frog: quality and intensity specification. *J Neurosci* 20: 2383–2390, 2000.

Dulac C, Wagner S. Genetic analysis of brain circuits underlying pheromone signaling. *Annu Rev Genet* 40: 449–467, 2006.

Dupuy F, Josens R, Giurfa M, Sandoz JC. Calcium imaging in the ant *Camponotus fellah* reveals a conserved odour-similarity space in insects and mammals. *BMC Neurosci* 11: 28, 2010.

Esslen J, Kaissling KE. Zahl und Verteilung antennaler Sensillen bei der Honigbiene (*Apis mellifera L.*). *Zoomorphology* 83: 227–251, 1976.

Ettlinger G. "Object vision" and "spatial vision": the neuropsychological evidence for the distinction. *Cortex* 26: 319–341, 1990.

Fernandez PC, Locatelli FF, Person-Rennell N, Deleo G, Smith BH. Associative conditioning tunes transient dynamics of early olfactory processing. *J Neurosci* 29: 10191–10202, 2009.

Free JB. *Pheromones of Social Bees*. Ithaca, NY: Comstock, 1987.

Friedrich RW, Korsching SI. Combinatorial and chemotopic odorant coding in the zebrafish olfactory bulb visualized by optical imaging. *Neuron* 18: 737–752, 1997.

Galizia CG, Franke T, Menzel R, Sandoz JC. Optical imaging of concealed brain activity using a gold mirror in honeybees. *J Insect Physiol*. 58: , 2012743–749.

Galizia CG, Joerges J, Küttner A, Faber T, Menzel R. A semi-in-vivo preparation for optical recordings of the insect brain. *J Neurosci Methods* 76: 61–69, 1997.

Galizia CG, McIlwrath SL, Menzel R. A digital three-dimensional atlas of the honeybee antennal lobe based on optical sections acquired by confocal microscopy. *Cell Tissue Res* 295: 383–394, 1999a.

Galizia CG, Menzel R. The role of glomeruli in the neural representation of odours: results from optical recording studies. *J Insect Physiol* 47: 115–130, 2001.

Galizia CG, Nägler K, Hölldobler B, Menzel R. Odour coding is bilaterally symmetrical in the antennal lobe of honeybees (*Apis mellifera*). *Eur J Neurosci* 10: 2964–2974, 1998.

Galizia CG, Rössler W. Parallel olfactory systems in insects: anatomy and function. *Annu Rev Entomol* 55: 399–420, 2010.

Galizia CG, Sachse S, Rappert A, Menzel R. The glomerular code for odor representation is species-specific in the honeybee *Apis mellifera*. *Nat Neurosci* 2: 473–478, 1999b.

Galizia CG, Vetter R. Optical methods for analyzing odor-evoked activity in the insect brain. *In Advances in Insect Sensory Neuroscience*, edited by Christensen TA. Boca Raton, FL: CRC, 2005, p. 349–392.

Ganeshina O, Menzel R. GABA-immunoreactive neurons in the mushroom bodies of the honeybee: an electron microscopy study. *J Comp Neurol* 437: 335–349, 2001.

Getz WM, Smith KB. Olfactory perception in honeybees: concatenated and mixed odorant stimuli, concentration and exposure effects. *J Comp Physiol A* 169: 215–230, 1991.

Giurfa M, Núñez JA. Honeybees mark with scent and reject recently visited flowers. *Oecologia (Berl)* 89: 113–117, 1992.

Grünewald B. Morphology of feedback neurons in the mushroom body of the honeybee, *Apis mellifera*. *J Comp Neurol* 404: 114–126, 1999.

Guerrieri F, Schubert M, Sandoz JC, Giurfa M. Perceptual and neural olfactory similarity in honeybees. *PLoS Biol* 3: 1–14, 2005.

Haddad R, Khan R, Takahashi YK, Mori K, Harel D, Sobel N. A metric for odorant comparison. *Nat Methods* 5: 425–429, 2008.

Haehnel M, Menzel R. Sensory representation and learning-related plasticity in mushroom body extrinsic feedback neurons of the protocerebral tract. *Front Syst Neurosci* 4: 161, 2010.

Hallem EA, Carlson JR. Coding of odors by a receptor repertoire. *Cell* 125: 143–160, 2006.

Hansson BS, Anton S. Function and morphology of the antennal lobe: new developments. *Annu Rev Entomol* 45: 203–231, 2000.

Hansson BS, Carlsson MA, Kalinovà B. Olfactory activation patterns in the antennal lobe of the sphinx moth, *Manduca sexta*. *J Comp Physiol A* 189: 301–308, 2003.

Hildebrand JG, Sheperd GM. Mechanisms of olfactory discrimination: converging evidence for common principles across phyla. *Annu Rev Neurosci* 20: 595–631, 1997.

Hourcade B, Muenz TS, Sandoz JC, Rössler W, Devaud JM. Long-term memory leads to synaptic reorganization in the mushroom bodies: a memory trace in the insect brain? *J Neurosci* 30: 6461–6465, 2010.

Hourcade B, Perisse E, Devaud JM, Sandoz JC. Long-term memory shapes the primary olfactory center of an insect brain. *Learn Mem* 16: 607–615, 2009.

Igarashi KM, Mori K. Spatial representation of hydrocarbon odorants in the ventrolateral zones of the rat olfactory bulb. *J Neurophysiol* 93: 1007–1019, 2005.

Joerges J, Küttner A, Galizia CG, Menzel R. Representations of odours and odour mixtures visualized in the honeybee brain. *Nature* 387: 285–288, 1997.

Johnson BA, Leon M. Chemotopic odorant coding in a mammalian olfactory system. *J Comp Neurol* 503: 1–34, 2007.

Johnson BA, Leon M. Local and global chemotopic organization: general features of the glomerular representations of aliphatic odorants differing in carbon number. *J Comp Neurol* 480: 234–249, 2004.

Johnson BA, Leon M. Modular representations of odorants in the glomerular layer of the rat olfactory bulb and the effects of stimulus concentration. *J Comp Neurol* 422: 496–509, 2000a.

Johnson BA, Leon M. Odorant molecular length: One aspect of the olfactory code. *J Comp Neurol* 426: 330–338, 2000b.

Kirschner S, Kleineidam CJ, Zube C, Rybak J, Grünewald B, Rössler W. Dual olfactory pathway in the honeybee *Apis mellifera*. *J Comp Neurol* 499: 933–952, 2006.

Knudsen JT, Tollsten L, Bergström LG. Floral scents: a checklist of volatile compounds isolated by head-space techniques. *Phytochemistry* 33: 253–280, 1993.

Kramer E. The orientation of walking honeybees in odour fields with small concentration gradients. *Physiol Entomol* 1: 27–37, 1976.

Kreher SA, Kwon JY, Carlson JR. The molecular basis of odor coding in the *Drosophila* larva. *Neuron* 46: 445–456, 2005.

Krofczik S, Menzel R, Nawrot MP. Rapid odor processing in the honeybee antennal lobe network. *Front Comput Neurosci* 2: 9, 2009.

Laska M, Teubner P. Olfactory discrimination ability for homologous series of aliphatic alcohols and aldehydes. *Chem Senses* 24: 263–270, 1999.

Lei T, Christensen A, Hildebrand JG. Spatial and temporal organization of ensemble representations for different odor classes in the moth antennal lobe. *J Neurosci* 24: 11108–11119, 2004.

Livingston MS, Hubel DH. Do the relative mapping densities of the magno- and parvocellular systems vary with eccentricity? *J Neurosci* 8: 4334–4339, 1988.

Malnic B, Hirono J, Sato T, Buck LB. Combinatorial receptor codes for odors. *Cell* 96: 712–723, 1999.

Marfaing P, Rouault J, Laffort P. Effect of the concentration and nature of olfactory stimuli on the proboscis extension of conditioned honey bees *Apis mellifera ligustica*. *J Insect Physiol* 35: 949–955, 1989.

Meister M, Bonhoeffer T. Tuning and topography in odor map on the rat olfactory bulb. *J Neurosci* 21: 1351–1360, 2001.

Mori K, Takahashi YK, Igarashi KM, Yamaguchi M. Maps of odorant molecular features in the mammalian olfactory bulb. *Physiol Rev* 86: 409–433, 2006.

Müller D, Abel R, Brandt R, Zöckler M, Menzel R. Differential parallel processing of olfactory information in the honeybee *Apis mellifera L. J Comp Physiol A* 188: 359–370, 2002.

Mustaparta H. Central mechanisms of pheromone information processing. *Chem Senses* 21: 269–275, 1996.

Nagao H, Yamaguchi M, Takahash Y, Mori K. Grouping and representation of odorant receptors in domains of the olfactory bulb sensory map. *Microsc Res Tech* 58: 168–175, 2002.

Ng M, Roorda RD, Lima SQ, Zemelman BV, Morcillo P, Miesenböck G. Transmission of olfactory information between three populations of neurons in the antennal lobe of the fly. *Neuron* 36: 463–474, 2002.

Pelz C, Gerber B, Menzel R. Odorant intensity as a determinant for olfactory conditioning in honeybees: roles in discrimination, overshadowing and memory consolidation. *J Exp Biol* 200: 837–847, 1997.

Polak EH. Multiple profile-multiple receptor site model for vertebrate olfaction. *J Theor Biol* 40: 469–484, 1973.

Rauschecker JP, Tian B. Mechanisms and streams for processing "what" and "where" in auditory cortex. *Proc Natl Acad Sci USA* 97: 11800–11806, 2000.

Reed CL, Klatzky RL, Halgren E. What vs. where in touch: an fMRI study. *Neuroimage* 25: 718–726, 2005.

Riffel JA, Lei H, Christensen TA, Hildebrand JG. Characterization and coding of behaviorally significant odor mixtures. *Curr Biol* 19: 335–340, 2009.

Robertson HM, Wanner KW. The chemoreceptor superfamily in the honey bee, *Apis mellifera*: expansion of the odorant, but not gustatory, receptor family. *Genome Res* 16: 1395–1403, 2006.

Roussel E, Sandoz JC, Giurfa M. Searching for learning-dependent changes in the antennal lobe: simultaneous recording of neural activity and aversive olfactory learning in honeybees. *Front Behav Neurosci* 4: 155, 2010.

Rubin BD, Katz LC. Optical imaging of odorant representations in the mammalian olfactory bulb. *Neuron* 23: 499–511, 1999.

Sachse S, Galizia CG. The role of inhibition for temporal and spatial odor representation in olfactory output neurons: a calcium imaging study. *J Neurophysiol* 87: 1106–1117, 2002.

Sachse S, Galizia CG. The coding of odour-intensity in the honeybee antennal lobe: local computation optimizes odour representation. *Eur J Neurosci* 18: 2119–2132, 2003.

Sachse S, Rappert A, Galizia CG. The spatial representation of chemical structures in the antennal lobe of honeybees: step towards the olfactory code. *Eur J Neurosci* 11: 3970–3982, 1999.

Sandoz JC. Odour-evoked responses to queen pheromone components and to plant odours using optical imaging in the antennal lobe of the honey bee drone *Apis mellifera L. J Exp Biol* 209: 3587–3598, 2006.

Sandoz JC, Galizia CG, Menzel R. Side-specific olfactory conditioning leads to more specific odor representation between sides but not within sides in the honeybee antennal lobes. *Neuroscience* 120: 1137–1148, 2003.

Sandoz JC, Deisig N, de Brito Sanchez MG, Giurfa M. Understanding the logics of pheromone processing in the honeybee brain: from labeled-lines to across-fiber patterns. *Front Behav Neurosci* 1: 5, 2007.

Schmuker M, Yamagata N, Nawrot MP, Menzel R. Parallel representation of stimulus identity and intensity in a dual pathway model inspired by the olfactory system of the honeybee. *Front Neuroeng* 17: 1–13, 2011.

Shearer DA, Boch R. Citral in the Nassanoff pheromone of the honey bee. *J Insect Physiol* 12: 1513–1521, 1965.

Snodgrass RE. *Anatomy of the Honey Bee*. Ithaca, NY: Comstock, 1956.

Stetter M, Greve H, Galizia CG, Obermayer K. Analysis of calcium imaging signals from the honeybee brain by nonlinear models. *Neuroimage* 13: 119–128, 2001.

Stopfer M, Jayaraman V, Laurent G. Intensity versus identity coding in an olfactory system. *Neuron* 39: 991–1004, 2003.

Strausfeld NJ, Lee JK. Neuronal basis for parallel visual processing in the fly. *Vis Neurosci* 7: 13–33, 1991.

Takahashi YK, Kurosaki M, Hirono S, Mori K. Topographic represenattion of odorant molecular features in the rat olfactory bulb. *J Neurophysiol* 92: 2413–2427, 2004.

Uchida N, Mainen Z. Odor concentration invariance by chemical ratio coding. *Front Syst Neurosci* 1: 1–6, 2007.

Uchida N, Takahashi YK, Tanifuji M, Mori K. Odor maps in the mammalian olfactory bulb: domain organization and odorant structural features. *Nat Neurosci* 3: 1035–1043, 2000.

Vareschi E. Duftunterscheidung bei der Honigbiene—Einzelzell-Ableitungen und Verhaltensreaktionen. *Z Vergl Physiol* 75: 143–173, 1971.

Vosshall LB, Wong AM, Axel R. An olfactory sensory map in the fly brain. *Cell* 102: 147–159, 2000.

Wang JW, Wong AM, Flores J, Vosshall LB, Axel R. Two-photon calcium imaging reveals an odor-evoked map of activity in the fly brain. *Cell* 112: 271–282, 2003.

Yamagata N, Schmuker M, Szyszka P, Mizunami M, Menzel R. Differential odor processing in two olfactory pathways in the honeybee. *Front Syst Neurosci* 3: 16, 2009.

Yamaguchi S, Wolf R, Desplan C, Heisenberg M. Motion vision is independent of color in *Drosophila*. *Proc Natl Acad Sci USA* 105: 4910–4915, 2008.

Zhao H, Ivic L, Otaki JM, Hashimoto M, Mikoshiba K, Firestein S. Functional expression of a mammalian odorant receptor. *Science* 279: 237–242, 1998.